Title
EROSION OF DUCTILE METALS BY SOLID PARTICLES

Author
Mcfadden, David.

Publication Date
1977-06-01

EROSION OF DUCTILE METALS BY SOLID PARTICLES

David McFadden
(M. S. thesis)

June 1977

Prepared for the U. S. Energy Research and
Development Administration under Contract W-7405-ENG-48

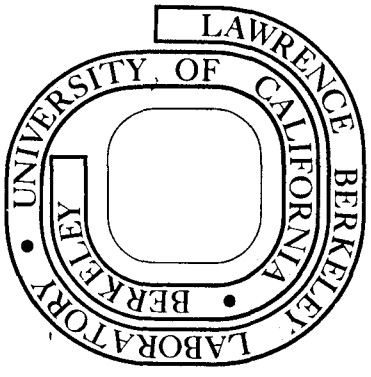

DISCLAIMER

LBL-6279

EROSION OF DUCTILE METALS BY SOLID PARTICLES

David McFadden

Materials and Molecular Research Division
Lawrence Berkeley Laboratory
and Department of Materials Science and Engineering
University of California
Berkeley, California 94720

June 1977

ABSTRACT

The present work was undertaken to study the mechanism involved in the erosion of ductile metals by solid particles at grazing angles of incidence. To investigate the material removal process, a series of multiple and single particle tests was conducted on 1100-0 aluminum with silicon carbide particles. These results were correlated with existing analytical models. Departures of the experimental results from theoretical predictions were resolved by considering a more realistic model of the erosion process.

TABLE OF CONTENTS

ACKNOWLEDGMENT

The author is grateful to Professor Iain Finnie for his guidance and help during the course of the investigation. Thanks are also due to Professors Shiro Kobayashi and Earl R. Parker for reviewing the manuscript.

The refurbishment and construction of the test apparatus by Mr. Walter Toutolmin is gratefully acknowledged.

This work was done under the auspices of the U. S. Energy Research and Development Administration.

I. INTRODUCTION

Through the years, erosion by solid particles in a fluid stream has been a problem in many industrial processes. Currently there is a great deal of interest in coal-hydrogenation. From pilot plant results and experience with similar operations, erosion appears to be an important, if not limiting, factor in the development of novel hydrogenation processes. The need for a better understanding of erosion in this connection is the motivation of the present work.

The study of erosion of ductile metals began in the 1930's. The first phase (1930~1960) of erosion research involved primarily the collection of erosion data for different materials and particles under varied conditions. This era defined the basic relationships involved in erosion and reported interesting observations on the erosion resistance of various metals and refractories. However, it was not until 1958 that the first analysis of erosion was performed. This study began the next phase of erosion work, that is, trying to develop an analysis to predict weight loss. An understanding of the basic mechanisms by which erosion occurs is necessary if predictions are to be made for new processes.

The first analysis of weight loss was given by Finnie,[1] who considered the erosion of an ideally ductile material by a hard angular particle as illustrated in Fig. 1. The basis of the analysis was the following assumptions:

(a) Material removal is the result of the cutting action of rigid particles.

(b) The plastic flow stress is constant.

(c) There is a constant ratio (k) between the horizontal and vertical forces acting on the particle during cutting.

(d) The volume removed is the product of the area swept out by the particle tip and the width (b) of the cutting face, $b \int_0^{t_c} Y_T dX_T$, where X_T and Y_T are the coordinates of the tip of the particle as shown in Fig. 1. The time at which cutting ceases is t_c.

(e) There are two conditions for which cutting may terminate. One possibility is that cutting ceases when the particle tip can no longer move forward ($\dot{X}_T(t_c) = 0$). The other case is when the particle leaves the surface while still cutting, that is, when the particle's tip has a horizontal velocity when $Y_T(t_c) = 0$.

(f) The area of contact is about twice the area given by the depth of cut ($L/y_t \cong 2$).

The two dimensional case shown in Fig. 1 was used as the basis of Finnie's analysis.[2] By solving the equations of motion of the tip of the particle, the volume removed was determined. The resulting expression for volume removal was found to be[3]

$$Vol = \frac{CmV^2}{4p\left(1+\frac{mr^2}{I}\right)} \left(\cos^2\alpha - \left(\frac{\dot{X}_T}{V}\right)^2\right) \qquad (1)$$

where Vol = volume swept out

m = mass of eroding particle

I = moment of inertia of particle about its center of gravity

r = radius of particle

C = fraction of particles cutting in idealized manner

α = angle of attack

V = particle velocity

p = horizontal component of pressure on particle taken equal to Vicker's Hardness H_V

$\dot{X}_T(t_c)$ = horizontal velocity of particle tip when cutting ceases

This expression when evaluated for the two possibilities for the end of cutting reduces to

$$Vol = \frac{CmV^2}{2p\left(1+\frac{mr^2}{I}\right)} \cos^2\alpha \quad ; \quad \dot{X}_T = 0 \qquad (2)$$

and

$$Vol = \frac{CmV^2}{4p\left(1+\frac{mr^2}{I}\right)} \left(\frac{2}{P}\right)\left[\sin 2\alpha - \frac{2\sin^2\alpha}{P}\right] \qquad (3)$$

where

$$P = \frac{k}{\left(1+\frac{mr^2}{I}\right)}$$

Finnie, et al,[3] conducted experiments in which weight loss as a function of angle of incidence, particle velocity, and target hardness were determined and correlated with predictions from the analysis.

For hard angular particles, SiC and Al_2O_3, it was found that the velocity exponent, n, varied from 2.04 to 2.50 rather than n = 2 as predicted. It was found that the analysis predicted an angle of attack for maximum erosion which was similar to experimental results. The general shape of the predicted and experimental erosion curves were found to be similar. Weight loss in erosion was found to vary inversely with Vicker's hardness of the surface for annealed metals. This indication of erosion resistance was also predicted by the analysis ($Vol \propto \frac{1}{H_V}$). It was found that heat treating steels or cold working other metals had little effect on the materials' erosion resistance.

In 1962 Bitter[4] proposed a theory for solid particle erosion which was based on Hertzian contact theory and assorted energy balances. Bitter categorized the process as consisting of two distinct mechanisms, cutting wear and deformation wear. He asserted that for ductile metals at low angles of attack, the cutting mechanism was predominant with negligible deformation wear and at high angles of attack deformation wear caused the majority of the damage. It should be noted that Bitter's approach was developed for both brittle and ductile erosion and that the only differences in these erosion mechanisms was the amount to cutting or deformation wear present.

Neilson and Gilchrist[5] presented Bitter's erosion analysis in the simplified form:

$$W = \frac{MV^2\cos^2\alpha\sin\alpha}{2\phi} + \frac{MV^2\sin^2\alpha}{2\varepsilon} \quad ; \quad \alpha < \alpha_0$$

and

$$W = \frac{MV^2\cos^2\alpha}{2\phi} + \frac{MV^2\sin^2\alpha}{2\varepsilon} \quad ; \quad \alpha > \alpha_0$$

where W = weight loss

M = total mass of eroding particles

V = particle velocity

α = angle of attack

α_0 = angle at which the horizontal component of particle velocity is zero

ϕ = the cutting energy absorbed by the surface to release one unit of eroded material

ε = deformation energy absorbed by the surface to release one unit of material

It is interesting to note that the final expressions have little if any relationship to the basis of the analysis.

Bitter[4] found by adjusting certain parameters in his analysis that Finnie's experimental results for aluminum and steel could be predicted. Neilson and Gilchrist[6] were also able to fit Bitter's analysis to their experimental work with some accuracy. Bitter's final weight loss equations are essentially a "curve" fit method and his predictions are highly dependent on the two empirical energy constants, ϕ and ε.

Winters and Hutchings[7] conducted studies with individual angular particles striking lead and steel samples to determine the relationship between the particle's orientation at the point of impact and the subsequent material damage. It was found that two different regimes of deformation existed, ploughing and cutting. They found that

ploughing occurred at large negative rake angles, that is, when the angle between the leading edge of the particle and the surface was small. Ploughing deformation was found to be reduced if the particle had some angular rotation while it was in contact with the surface. At more positive rake angles, cutting deformation occurred, but its effectiveness was reduced by any rolling of the particle. This rolling action resulted in the particle penetrating deeply into the surface rather than sweeping though the material. The authors also observed localized deformation, identified as adiabatic shear bands, in the lips raised during cutting deformation.[7,8] They suggested that materials susceptible to adiabatic shear may also have a lesser resistance to erosion.

Tilly[9] proposed a completely different two stage process for the erosion mechanism. This consisted of a primary and secondary process rather than two mechanisms which dominate under different conditions of rake angle and angle of attack. These two stages were identified as:

(a) Primary erosion starts with the indentation of the surface followed by a micromachining process for chip removal.

(b) The second stage consists of impacting particles fracturing and the resulting fragments producing additional removal. Tilly tried to support this mechanism by characterizing the particles size distribution and relating the size change to the observed erosion.

The studies by Goodwin, et al,[18] showed interesting variations in erosion parameters with particle size and base material. The velocity

exponent was found, for small particles, to be 2 but for sizes above ~100 μm it was approximated as 2.3 for normal impacts. These tests were conducted on several ductile materials. Tilly and Sage[17] found a dependence of erosion rate on particle diameter for a given impact velocity. They found for a number of ductile materials that the results, weight loss as a function of particle diameter, could be divided into three regions. These areas consisted of a segment defined by a threshold diameter (d_{EL}) below which no erosion occurred, a region above d_{EL} where weight loss has a power law relationship to the diameter, and for still larger particles the erosion rate was constant.

Experiments relating the erosion characterists of single and multiple particle impacts were conducted by Sheldon and Kanhere.[11] These tests consisted of the erosion of 6061 aluminum (annealed and work hardened) by large diameter stell and glass shot (dia. ~2500 μm) at angles of incidence of 20 and 90 degrees. The velocity exponent (n) determined for single and multiple particle tests were similar. For work hardened aluminum at $\alpha = 20°$, the velocity exponent was approximately 2.8. The annealed specimen under similar conditions produced a velocity exponent which varied from 2.3 to 2.4.

Sheldon and Kanhere[11] developed an erosion model based on the materials' indentation hardness characteristics. The derivation, for normal impact only, consisted of a simple energy balance between the kinetic energy of the particle and the work expended during indentation. This approach produced a weight loss prediction of the form

$$W \cong \frac{D^3 V^2 (\rho)^{3/2}}{H_V^{3/2}} \qquad (4)$$

where D = particle diameter

V = particle velocity

ρ = particle density

H_V = Vicker's hardness

W = weight loss

The model assumed that the force necessary to indent the surface was proportional to the depth of penetration to a power m, somewhat like a "dynamic" hardness test, but it did not consider the strain harding of the surface or the inertia of the particle. Sheldon and Kanhere contend that the exponent for velocity (n = 3) is close to the actual experimental values. However, the prediction that the weight loss was proportional to $H_V^{-3/2}$ is in disagreement with experimental results.

Sheldon[12] maintained that the best material property for correlation with erosion wear is the hardness value of the target material in the fully work hardened condition as measured on the damaged surface. It was found, for a number of pure materials, that the hardness was as much as five times higher than that measured for the annealed material. Sheldon proposed that the fully work hardened value for hardness should be used in analyses which employ a particle cutting or material displacement mechanism for material removal.

Based on the preceding literature review it appears that different erosion mechanisms predominate at low and high angles of impingement.

Since low or grazing angles lead to the largest volume removal it was decided to concentrate on this aspect of erosion.

As a starting point we will investigate the model for solid particle erosion proposed by Finnie.[1,2] At the present time, this is the only theory which attempts to explain the erosion process. The theories proposed by Bitter or Neilson and Gilchrist seem to be little more than a curve fit, and those presented by Tilly, Sheldon, etc., are composed mostly of observations with very little modeling of the process.

The work that will be described involved experiments with both single and multiple impacts. These results are compared with those predicted analytically. Departures from the predicted behavior are considered and a modified analysis of erosion at grazing angles is developed.

II. EXPERIMENT

The tests were made with an erosion testing device originally developed by Sheldon.[13] The equipment was subsequently modified for velocity measurement and easier operation. In its final form it is shown in Figs. 2 and 3.

The basic operation of the tester is simple and effective. The silicon carbide was fed into the air stream, mixed for uniform particle distribution, and then propelled down the tube by the air flow. By varying the pressure drop across the nozzle, the air and particle velocity could be controlled. It was found that the particle velocity was a function of the inner diameter of the tube, the loading factor (grams of particles/grams of air), the pressure drop across the nozzle, the surface roughness of the nozzle, and the size and shape of the particles. To ensure constant velocities during tests, the above parameters must be kept as constant as possible.

For multiple particle tests, the hopper feed arrangement shown in Fig. 3 was used. This arrangement provided a very satisfactory means of depositing the particles into the air stream at a constant rate. The mass of particles entering the air stream was a function of the hopper rake angle (Δ) and the air pressure applied to the hopper vibrator.

For the single particle tests, consisting of five particles impacting the target, the hopper was replaced by a glass and plastic tube device, and the larger particles were fed from the tube into the

mixing chamber. A constant loading factor was not needed to ensure a constant velocity in that at such small loadings any small deviation of this value had negligible effect on the particle velocity.[14]

To determine the particle velocity, the rotating disc device shown in Fig. 4 was employed. This equipment was based on the design of Ruff and Ives.[15] To determine the particles' velocities, the parameters (R, S, L, V) shown in Fig. 4b were needed. The simple observation that the time it takes the particle to travel between the discs is equal to the time it takes the disc to rotate through the arc length was required.

There are several advantages of the rotating disc method when compared to a double flash photographic system. The strong points of the rotating disc are that it is less expensive to build and operate, it gives very accurate results, and less time is needed for particle velocity calibration. Its accuracy is due to the large number of particles which are used during a test and the resulting averaging of variations in operating conditions (particle orientation in the stream, particle loading, particle size). For several tests, at a given set of conditions, this method produced results which varied by less than 5%.

All but a few experiments used silicon carbide particles and 1100-0 aluminum targets. The choice of these materials was dictated by availability and the fact that an extensive amount of previous testing had been carried out with this combination. Specimens were prepared from sheared plates by polishing with silicon carbide abrasive

papers starting at 240 grit and ending at 600 grit. For the multiple particle tests in which weight loss was determined as a function of velocity, angle of attack, and amount of abrasive, the silicon carbide particles had a size range between 48 and 62 mesh (250-300 μm). This size range corresponds to a weight equivalent spherical particle of 280 μm diameter. The purpose of the single particle experiments was to make observations on the craters formed during impact. To make the observations easier, larger, 12 to 16 mesh, silicon carbide particles were used. These particles had equivalent diameters of 1100 μm.

III. RESULTS

A. Qualitative Interpretation of Single Particle Impacts

A large number of single particle impacts were examined with the scanning electron microscope. It is not possible to present all of these so representative photographs are shown in Figs. 5-11. These stereo pairs (10° tilt) provide a graphic picture of the mechanisms involved in erosion. To supplement the photographs, a profile through the approximate centerline of the crater is also shown.

Figures 5 through 7 are craters that were formed by particles which had angles of incidence of 10, 11, and 15 degrees, respectively. These craters had similar characteristics in that each exhibits, to some degree, striation from the cutting edge of the particle, a lip at the end of the crater, and were shallow with an average length to depth ratio of about 10. At 10 degrees, the particle swept though the surface and removed the majority of the displaced material. The 11° and 15° impacts are similar in that the particles entered the surface in a cutting manner. However, in these cases the particles were unable to remove all of the displaced material and left a large lip of material at the end of the craters.

A transition in the removal mechanism appears to occur between 20 and 40 degrees. In this area, a change from a cutting mechanism of removal to one involving indentation appears to take place. The 20° and 30° impacts (Figs. 8 and 9) are typical of this region in that the particle entered the surface in a cutting manner and proceeded to plough the material forward. In this region, there is considerable

displaced material and the craters are becoming shorter and deeper compared to the grazing impacts (10°-20°) with length to depth ratio of about 5.

At higher angles of incidence (40°-90°) the deformation mechanism is primarily one of indentation with very little cutting occurring. Figure 10 shows a crater formed at 60 degrees. The particle indents the surface as it moves across it with the resulting damage being the depression of the surface. The original surface can be seen on the floor of the crater. At 90°, Fig. 12, the damage is the result of surface indentation by the particle. As with the 60° crater, the 90° impact has only minor material displacement at the edges of the crater, and the crater floor has a remarkably constant slope.

B. Cutting Analysis

To determine the applicability of Finnie's cutting theory, a series of experiments were conducted. Since the single particle tests showed that a cutting type removal mechanism was appropriate over a range of $10 < \alpha < 30°$, the correlations between predictions and experimental results will be confined to this region. The theory and tests results were examined for the following cases:

(i) Multiple particle tests were compared to the predictions of Eq. 1.

(ii) Crater profiles obtained from the single particle experiments and profiles predicted from the analysis were compared. Also, an estimate of the material hardness (H_V) was obtained from single impacts and the analysis.

(iii) The assumptions made for several of the parameters (e.g. k) in the analysis were compared to the test results.

Erosion (expressed as g removed/g abrasive) as a function of the angle of incidence, for particle velocities of 77 m/s and 102 m/s, is shown in Fig. 12. By examining the normalized curves, it can be seen that the maximum amount of weight loss occurs at about 11° for the lower velocity and 12° for the higher, and that erosion curves have very similar shapes between 10 and 30 degrees but diverge after that point. (It is interesting to note that at 90°, for the lower velocity test, the erosion is 13% of the maximum, while at 107 m/s the erosion is about 22% of the peak value.) The velocity exponents for the expression erosion α V^n, plotted on Fig. 12, range from 2.46 at 10 degrees to 3.12 for normal impacts.

A comparison of Finnie's analysis using Eq. 1 and the experimental results is shown in Fig. 13 (normalized about their peak weight loss values). Using Finnie's assumptions for the constants $k = 2$, $\frac{I}{mr^2} = 3$, the results compare favorably for what we have termed the cutting region. For both velocities, the shape of the experimental curve and predicted curve are very similar in the region of $\alpha < 30°$, and the analysis predicts a peak erosion angle very similar to the test results. As would be expected, the cutting analysis and the experimental results diverge for higher angles.

There are several anomalies in the cutting analysis when compared to experimental results. The analysis predicts a constant velocity

exponent of 2, whereas the experimental results show an exponent which is greater than 2 and increases with α. These aspects are discussed in detail in section C.

By plotting the erosion results in terms of erosion per particle for both experimental and analytical results (Fig. 14), it is possible to make an estimation of the cutting efficiency. Using the values of annealed hardness for the horizontal stress p, a cutting efficiency of one, and an average particle weight, the analysis underestimates the test results by about a factor of 10.5. This result is similar to Finnie's[1] assertion that the cutting efficiency for erosion should be similar to the efficiency found in abrasive wear studies, that is, 1 particle in 10 produces actual removal while the remainder displace and roughen the surface.

On the other hand, Sheldon[12] contends that eroding particles work harden a surface to about five times the annealed hardness. In this case the discrepancy between experimental and analysis is a factor of about two. In other words about half of the particles would then be cutting in the idealized manner. It is difficult to isolate the variables C and p in Eq. 1 but their quotient $\frac{C}{p}$ seems to be approximately $\frac{0.1}{H_V}$ when annealed metals are eroded by silicon carbide grains. We will later present some evidence to support the viewpoint that p should be taken as the Vickers hardness H_V.

The trajectory of the particle's tip, X_T and Y_T, as it cuts through the surface was predicted using Finnie's analysis. These results were compared to the profiles of typical single impacts.

Finnie[1] showed in his original paper that the motion of the particle's tip can be described as with reference to Fig. 1 as:

$$Y_T = Y \tag{5}$$

$$X_T = X + r\phi \tag{6}$$

where

$$Y = \frac{V\sin\alpha}{\beta} \sin\beta t$$

$$X = \frac{V\sin\alpha}{k\beta} \sin\beta t + V\cos\alpha(t) - \frac{V\sin\alpha}{k}(t)$$

$$\phi = \frac{mr\ V\sin\alpha}{kI\ \beta} [\sin\beta t - \beta t]$$

$$\beta = \left(\frac{Pk\psi b}{m}\right)^{1/2}$$

Then expressing equations 5 and 6 in a dimensionless form, X^* and Y^*, the particle's trajectory is shown to be

$$X^* = \frac{\beta X_T}{V} = \sin\tau(2\sin\alpha) - \tau(2\sin\alpha) + \tau(\cos\alpha) \tag{7}$$

$$Y^* = \frac{\beta Y}{V} = \sin\alpha\ \sin\tau \tag{8}$$

where $\tau = \beta t$, $I = 1/3\ mr^2$ and $k \cong 2$.

A comparison of profiles predicted by Eqs. 7 and 8 and several typical single impacts are shown in Figs. 15 and 16. The curves are scaled such that the maximum depth of cut for the analysis and the test results are the same.

For an angle of 10 degrees the analysis predicts the general shape of the crater quite well, The positions of the maximum depth of cut (Y^*_{max} at $X^* = 1.2$) are similar as is the trajectory of the particle before it reaches Y^*_{max}. There is some dissimilarity near the end of

the volume removal process in that, in two of the actual cases, the particle travels a bit further but raises a small lip. The analysis shows the particle covering a shorter horizontal distance but removing the entire volume.

Even at the limits of the cutting region ($\alpha \cong 30°$), the analysis is able to describe many of the features of the actual impact. The trajectory of the particle's motion for the predicted and experimental cases is similar up to the maximum depth of cut. After Y^*_{max} the comparison of the analysis and impact results is no longer valid. The analysis assumes that the particle removes all of the material up to Y^*_{max} and is then ejected from the surface. In reality, the particle displaces extra material past Y^*_{max} to create a large lip on the leading edge of the crater.

There is, of course, variability from one impact to another with angular particles so one should not expect precise predictions from an idealized model.

It was also of interest to determine whether the cutting theory could predict the plastic flow stress which a single particle would "see" during the removal process. By using the non-dimensional parameter Y^* and several dimensions from the single particle experiments, a "flow pressure" could be estimated and compared to the material hardness H_V.

From the cutting theory it is shown that

$$Y^* = \frac{\beta Y}{V}$$

or for the maximum depth, Y_{max},

$$\frac{\beta_{max} Y_{T_{max}}}{V} = \sin\alpha \qquad (9)$$

Solving the above relationship for β_{max} yields

$$\beta_{max} = \left(\frac{Pk\psi b}{m}\right)^{1/2} = \frac{V}{Y_T} \sin\alpha \qquad (10)$$

where m = mass of particle

k = force ratio = 2

p = flow pressure

ψ = $L/Y_T \cong 2$

b = width of impact

The maximum flow pressure is then expressed as

$$P_{max} = \frac{mV^2 \sin^2\alpha}{Y^2_{T_{max}} 4b} \qquad (11)$$

By taking measurements for $Y_{T_{max}}$ and b and knowing the velocity, mass, and angle α, the flow stress for the single particle impacts at 10, 15, 30, and 60 degrees (Figs. 5, 7, 9, 10) could be determined. The results of this prediction are presented in Fig. 17 and are comparable to the actual hardness which the single particles "saw" on impact, that is, the hardness of the fresh aluminum surface ($H_V \cong 28$ kg/mm^2). It is interesting, although perhaps coincidental, to note that by extrapolating the results of Fig. 17 to $\alpha = 0°$, the hardness obtained is approximately equal to the value for the annealed specimen.

The average ratio of horizontal to vertical forces, k, was determined experimentally to be 2.12 (k = 2 in analysis). This experiment consisted of several angular particles (1400 μ dia. SiC) being mounted on styluses and the recording of the horizontal and vertical forces which the particles generated as they scratch the 1100-0 aluminum specimen.

Some of the assumptions of the cutting analysis can be verified by the experimental results already presented. It was assumed that the particle entered the surface at the angle of incidence of the air stream to the specimen. By measuring the initial slope of the particle's trajectory for single particle tests, it was found that for $\alpha < 40°$ the average slope deviates from the assumed angle of incidence by less than 7%. For the cutting region, only two modes of cutting are observed, that is, the particle was able to leave the surface in a cutting manner ($Y_T(t_c) = 0$) or the forward motion of the particle was stopped by the base material ($\dot{X}_T(t_c) = 0$). The lack of secondary damage in single particle tests indicates that the particle is rigid and did not fracture upon impact as was assumed in the analysis.

By using Figs. 18 and 19, the assumption that for multiple impacts the flow pressure each particle "sees" is the annealed hardness (H_v) of the base metal is shown to be reasonable. The results, represented as two linear regions with positive increasing slopes, indicate that the particle "sees" a constant hardness in the steady state region. This pressure must be similar to the annealed hardness observed in the

incubation portion of the results in that the erosion rate had increased somewhat when compared to the initial rate. If it is assumed the particles see a progressively work hardened surface, then the erosion rate should decrease with the amount of abrasive and not increase as the results indicate. It is noted that the transition from the incubation portion of the curve to the steady state region (e.g. 180 gm at 27 $\frac{m}{s}$) is characterized by the onset of rippling.

C. Modification of the Cutting Analysis

In view of the success of the cutting analysis in explaining many features of erosion at low angle of impingement, it is disturbing that it underestimates the velocity exponent. As pointed out earlier the theoretical value of 2 in the relation volume $\sim V^n$ is rarely observed with experimental values ranging from 2.4 to 2.6 or greater. Other than the Sheldon and Kanhere[11] model based on indentation (Eq. 4) which predicts volume $\sim V^3$ and Tilly's suggestion[9] that shattering and secondary erosion occur at higher velocities, there has been little attention paid to this discrepancy. Both of these approaches are lacking in generality and clearly do not apply to the experiments we have reported.

One consideration is that the thermal properties of the eroded surface may be involved in the mechanism of erosion. This was disposed of by testing titanium. Its thermal diffusivity (.0282 cm^2/sec) differs greatly from that for aluminum (.712 cm^2/sec). However, the values for

the exponent n were essentially the same as for aluminum ($n_{Al} = 2.42$, $n_{Ti} = 2.47$ at $\alpha = 10°$ and velocities of 39 and 97 $\frac{m}{s}$).

In searching for another explanation, Finnie[16] examined the assumptions of his original analysis. He suggested that the equation for angular rotation be modified to locate the resultant force at the correct distance from the C.G. of the particle. Originally this was taken to act at the tip of the particle since this simplified the analysis. However, as shown in Fig. 20 it is more realistic to locate the resultant force in the center of the material having contact with the particle. The symmetrical picture of two-dimensional cutting shown in the figure could be considered as an average condition for grains which are "tilted" in either direction as they strike the surface.

The equations of motion for the X and Y ($Y_T \cong Y$) directions are unchanged by this modification and are

$$m\ddot{X} + P_Y \psi b = 0 \tag{12}$$

$$m\ddot{Y} + kpY\psi\, b = 0 \tag{13}$$

The equation for angular rotation now becomes:

$$I\ddot{\phi} + P\psi b(r-Y)Y - 2p\psi\,(Y)^2 bk = 0 \tag{14}$$

where $p\psi bY$ = horizontal force

$p\psi Ybk$ = vertical force

The assumptions used in the above equations are identical to those used in the original analysis.

Solving Eq. 13, the vertical motion of the particle can be expressed as

$$Y(t) = c_1 \sin\beta t + c_2 \cos\beta t \tag{15}$$

where

$$\beta = \left(\frac{Pk\psi b}{m}\right)^{1/2} \tag{15}$$

using the initial conditions that at $Y(0) = 0$ and $\dot{Y}(0) = V\sin\alpha$ the expression for $Y(t)$ reduces to

$$Y(t) = \frac{V}{\beta} \sin\alpha \sin\beta t \tag{16}$$

Substituting $Y(t)$ into Eq. (12), the horizontal motion of the particle is found to be

$$X(t) = \frac{V\sin\alpha}{k\beta} \sin\beta t + c_1 t + c_2 \tag{17}$$

For the boundary conditions $X(0) = V\cos\alpha$ and $X(0) = 0$, $X(t)$ may be expressed as:

$$X(t) = \frac{V\sin\alpha}{\beta k} \sin\beta t + \left\{V\cos\alpha - \frac{V\sin\alpha}{k}\right\} t \tag{18}$$

The rotation of the particle is found to be of the form

$$\phi(t) = \left\{\frac{P\psi b}{I}\right\}\left[\left\{\frac{dV^2\sin\alpha^2}{\beta^2}\right\}\left(\frac{1}{4} t^2 + \frac{1}{8\beta^2}\cos 2\beta t\right)\right.$$

$$\left. + \frac{rV\sin\alpha}{\beta^3} \sin\beta t - \frac{rV\sin\alpha}{\beta^2} - \frac{d^2V^2\sin^2\alpha}{8\beta^2}\right] \tag{19}$$

where $d = 2k + 1$ and the other constants are as defined previously. It is assumed that for many impacts the initial particle rotation and angular velocity would, on the average, be zero ($\phi(0) = \dot{\phi}(0) = 0$). If it is assumed that $I = \frac{1}{3} mr^2$ and $k = 2$ for angular particles, then

$$\phi(t) = \frac{15}{16} \frac{V^2\sin^2\alpha}{\beta^2 r^2}\left[2(\beta t)^2 + \cos 2\beta t - 1\right] + \frac{3}{2} \frac{V\sin\alpha}{2r\beta} (\sin\beta t - \beta t) \tag{20}$$

As in the original analysis, the motion of the particle's tip can be expressed as

$$Y_T \cong Y$$

and

$$X_T \cong X + r\phi$$

Again, this assumption implies an average condition exists for many impacts. Since the motion of the particle's tip is known, then the volume removed is

$$\text{Vol} = b \int_0^{t_c} Y_T \dot{X}_T \, dt \tag{21}$$

where t_c = time at which cutting ceases

b = a unit width of the cutting face

Combining Eqs. 16, 18 and 20, the volume expression reduces to

$$\frac{\text{Vol}}{b} = \frac{V\sin\alpha}{\beta} \int_0^{t_c} (\sin\beta t) \left[(A_2 - A_3 - A_7) + (A_1 + A_6)\cos\beta t - A_5 \sin\beta t + A_4 t\right] dt$$

where $A_1 = \frac{V}{2}\sin\alpha$

$A_2 = V\cos\alpha$

$A_3 = \frac{1}{2} V\sin\alpha$

$A_4 = \frac{15}{4} \frac{V^2}{r} \sin^2\alpha$

$A_5 = \frac{15}{8} \frac{1}{r\beta} V^2 \sin^2\alpha$

$A_6 = \frac{3}{2} V\sin\alpha$

$A_7 = A_6$

Evaluating the integral from 0 to t_c, the volume expression is

$$\frac{Vol}{b} = \frac{V^2\sin^2\alpha}{\beta^2}\left[\cos\beta t_c(2 - \cot\alpha) + \cot\alpha - \frac{3}{2} - \frac{1}{2}\cos 2\beta t_c\right] + \frac{V\sin\alpha}{\beta}\left[\frac{A_5}{\beta}\left(-\frac{1}{2}\sin\beta t_c + \frac{1}{6}\sin 3\beta t_c\right) + A_4\left(\frac{1}{\beta^2}\sin\beta t_c - \frac{1}{\beta}t_c\cos\beta t_c\right)\right] \quad (22)$$

This expression is composed essentially of Finnie's original solution (the first parentheses) and a correction term.

To determine the volume removal for the case when the tip of the particle is still moving horizontally as it leaves the surface, the condition on t_c is that $Y(t_c) = 0$ when $\dot{X}_T$ exists or $\beta t_c = \pi$. Using this condition, the expression is given as

$$\frac{Vol}{b} = \frac{V^2}{\beta^2}(\sin 2\alpha - 4\sin^2\alpha) + \frac{15}{4}\pi\frac{V^3\sin^3\alpha}{r\beta^3} \quad (23)$$

The other possibility for the manner in which the particle ceases to remove material is when it is prevented from moving through the surface, that is, when $\dot{X}_T(\beta t_c) = 0$. This condition for cutting termination can be expressed as

$$V\cos\alpha - 2V\sin\alpha + 2V\sin\alpha\cos\beta t_c - A_5\sin(2\beta t_c) + \frac{A_4}{\beta}(\beta t_c) = 0 \quad (24)$$

By combining this expression and Eq. 22, the volume removed for this region is given as

$$\frac{Vol}{b} = \frac{V\sin\alpha}{\beta}\left[\frac{V\cos\alpha}{\beta} - \frac{V\sin\alpha}{\beta}\sin^2\beta t_c + \frac{V^2\sin^2\alpha}{8\beta^2 r}(15\sin\beta t_c - 5\sin 3\beta t_c)\right] \quad (25)$$

It is noted that t_c, as determined from Eq. 24, is a function of the angle α and must be determined for each angle of impingement.

Since maximum erosion occurs when the particle leaves the surface while still cutting, the implications of Eq. 23 will be considered first.

If we assume that for two velocities V_2 and V_1 the volume removal can be expressed as Volume α V^n, then a value n may be estimated from Eq. 23. Recalling that $\beta^2 = pk\psi b/m$, then

$$\frac{Vol_{V_2}}{Vol_{V_1}} = \left(\frac{V_2}{V_1}\right)^n = \left(\frac{V_2}{V_1}\right)^2 \frac{\left(\sin 2\alpha - 4\sin^2\alpha + \frac{15}{4}\pi \frac{V_2 \sin^3\alpha}{\beta r}\right)}{\left(\sin 2\alpha - 4\sin^2\alpha + \frac{15}{4}\pi \frac{V_1 \sin^3\alpha}{\beta r}\right)}$$

Since $Y_{max} = \frac{V\sin\alpha}{\beta}$ the last term in parentheses becomes $\frac{15}{4}\pi \frac{Y_{max}}{r}$. If an estimate can be made for $\frac{Y_{max}}{r} = \lambda$ for V_1, then $\left(\frac{Y_{max}}{r}\right)$ for $V = V_2$ is merely $\left(\frac{V_2}{V_1}\right)\lambda$. The preceding equation becomes

$$\left(\frac{V_2}{V_1}\right)^{n-2} = \frac{\sin 2\alpha - 4\sin^2\alpha + \frac{15}{4}\pi \frac{V_2}{V_1}\lambda \sin^2\alpha}{\sin 2\alpha - 4\sin^2\alpha + \frac{15\pi}{4}\lambda \sin^2\alpha} \qquad (26)$$

Typically in erosion tests at two velocities used to determine the exponent n the value of λ is about 0.1. The following table shows n values calculated from the preceding equation for three velocity ratios as well as values for λ = .075 and .125.

Table 1. Velocity exponents as determined from Eq. 26 for several angles, velocity ratios, and λ = .125, .100 and .075.

		Velocity Exponent n		
λ	$\frac{V_2}{V_1}$	$\alpha = 11°$	$\alpha = 15°$	$\alpha = 18°$
.125	2	2.250	2.377	2.492
	1.75	2.237	2.261	2.457
	1.5	2.224	2.343	2.436
.100	2	2.212	2.326	2.420
	1.75	2.198	2.311	2.402
	1.5	2.186	2.294	2.368
.075	2.	2.168	2.267	2.358
	1.75	2.158	2.253	2.358
	1.50	2.148	2.239	2.333

While these values are somewhat smaller than the experimental results presented previously, they are in the range reported by Finnie[1] and Tilly.[9] The results also indicate that the exponent n increases with the angle α, as do the experimental results of Fig. 12 and those of Sheldon.[11] Varying λ and V_2/V_1 has little effect on the velocity exponent at a given angle with a maximum change of n of less than 6%.

Up to this point we have discussed only the effective velocity exponent for the situation of the particle leaving the surface while still cutting, but it is of interest to determine n for the case when the particle is prevented from moving through the surface. For the case of $\lambda = 0.1$, the transition between the two conditions occurs at 21°, a higher value than given by the simple analysis. The end of the cutting region ($\alpha \cong 30°$) will be considered. Solving Eq. 24 for the time at which cutting ceases (βt_c) and then evaluating Eq. 22, the effective veolcity exponent n for $\alpha = 30°$, $V_2/V_1 = 2$, and $\lambda = .1$ was found to be 2.76 which is very similar to experimental results.

The modified analysis does predict a shift in the peak angle of erosion with velocity. Differentiating Eq. 23 with respect to α, the relationship for the peak erosion is found to be

$$\tan 2\alpha = \frac{1}{2 - \frac{30}{16}\pi\left(\frac{V_2}{V_1}\right)\lambda} \qquad (27)$$

Evaluating Eq. 27 for velocities V_1 and $1.4V_1$, and assuming for typical impacts that $\lambda = .1$, then the peak erosion angles are

$$\alpha_1 = 17.76^\circ; \qquad V = V_1$$

$$\alpha_2 = 20.21^\circ; \qquad V = 1.4V_1$$

Determining the exact angle for peak erosion is very difficult, and trying to find such slight shifts in the peak value would require extensive experiments.

One of the features of the original analysis is its ability to predict the shape of single particle impacts, and it is necessary to determine if the new analysis predicts similar profiles. As before the nondimensional parameters X^* and Y^* are used for profile determination and take the form of

$$X^* = 2\sin\alpha\sin\beta t + (\cos\alpha - 2\sin\alpha)\beta t + \frac{1.5}{16} V\sin\alpha\,(2(\beta t)^2 - \cos 2\beta t - 1) \tag{28}$$

$$Y^* = \sin\alpha\sin\beta t \tag{29}$$

where $\lambda = .1$. A comparison between the experimental profiles, those obtained from the original analysis, and those of the modified analysis are presented in Fig. 21. The new analysis predicts the crater profile somewhat more accurately than the original theory at 10°, but there is little difference in the results at 30°.

IV. CONCLUSION

The assumption in solid particle erosion that the particle removes material in a cutting manner was found to be valid for an angle of incidence of less than 30°. The basic model proposed by Finnie[1] was found, to a large extent, to describe the erosion process for this region. By making this model more realistic, some of the erosion characteristic were more precisely described.

Single particle experiments indicate the erosion process for $\alpha < 30°$ was primarily one of cutting, and for $\alpha > 40°$ the erosion process was predominately one of indentation. At angles between 20° and 40° degrees (a transition region) the mechanism for removal was a combination of cutting and indentation deformation.

Finnie's original analysis was able to predict many of the erosion characteristics of multiple and single particle damage. It was found to be very effective for multiple particle tests for $\alpha < 30°$, but for larger angles of incidence the experimental and predicted results diverged. Also, the cutting analysis was able to predict some of the features, crater profiles and the flow stress, of single particle impacts at $\alpha < 30°$. Both single and multiple impacts were used to confirm assumptions used in the analysis. It was shown that the assumptions for the force ratio k, the geometric parameters, and for treating the particle as rigid were valid. The proposal was made that the Vicker's hardness of the annealed specimen best described the surface that both multiple and single particles "see" on impact. Using this assumption

for the flow stress, then the cutting efficiency was shown to be about .1 for multiple particle tests.

By modifying the original analysis, the discrepancy in predicting the role of velocity could now be explained. The modified cutting analysis produced an effective velocity exponent ranging from $\sim$2.2 at 10° to $\sim$2.7 at 30°. These results are similar to reported experimental results, that is, the exponent n is in the range of 2.2 to 2.8 and n increases with the angle of impingement α. A small shift in the peak angle of erosion with velocity is also predicted, but it was not distinguishable in the experiments. Also, the profiles for single impacts were predicted more accurately than before for $\alpha < 30°$

REFERENCES

1. I. Finnie, "The Mechanism of Erosion of Ductile Metals", Proc. 3rd U.S. Natl. Congr. Appl. Mech., (1958).

2. I Finnie, "Some Observations on the Erosion of Ductile Metals", Wear 19, 81-90 (1972).

3. I. Finnie, J. Wolak, Y. Kabil, "Erosion of Metals by Solid Particles", Journal of Materials 2, No. 3, 682-700 (1967).

4. J. G. A. Bitter, "A Study of the Erosion Phenomena", Parts 1 and 2, Wear 6, 5, 1969 (1963).

5. J. H. Neilson and A. Gilchrist, "Erosion by a Stream of Solid Particles", Wear 11, 111-122 (1968).

6. J. H. Neilson and A. Gilchrist, "An Experimental Investigation into Aspects of Erosion in Rocket Motor Tail Nozzles", Wear 11, 123-143 (1968).

7. I. M. Hutchings and R. E. Winter, "Particle Erosion of Ductile Metals: A Mechanism of Material Removal", Wear 27, 121-128 (1974).

8. R. E. Winter and I. M. Hutchings, "The Role of Adiabatic Shear in Solid Particle Erosion", Wear 34, 141-148 (1975).

9. G. P. Tilly, "A Two Stage Mechanism of Ductile Metals", Wear 23, 87-96 (1973).

10. G. P. Tilly, "Sand Erosion of Metals and Plastics: A Brief Review", Wear 14, 241-248 (1969).

11. G. L. Sheldon and A. Kanhere, "An Investigation of Impingement Erosion Using Single Particles", Wear 21, 195-209 (1972).

12. G. L Sheldon, "Effects of Surface Hardness and Other Material Properties on the Erosion Wear of Metals by Solid Particles", Trans. A.S.M.E. 99H, 133-137 (1977).

13. G. Sheldon, "Erosion of Brittle Materials", Ph.D. Thesis, University of California, Berkeley, Ca.

14. D. Kleist, "One Dimensional – Two Phase Flow", M.S. Thesis, University of California, Berkeley, Ca.

15. A. W. Ruff and L. K. Ives, "Measurement of Solid Particle Velocity in Erosive Wear", Wear 35, 195 (1977).

16. I. Finnie, Personal Correspondence.

17. G. P. Tilly and Wendy Sage, "The Interaction of Particle and Material Behavior in Erosion Process", Wear 16, 447-465 (1970).

18. J. E. Goodwin, W. Sage, C. P. Tilly, "Study of Erosion by Solid Particles", Proc. Inst. Mech. Engrs. 184 (15), 279-292 (1969).

FIGURE CAPTIONS

Fig. 1. (A) Two-dimensional picture of an angular particle surface material. (B) The forces acting on a particle during the removal process.

Fig. 2. A photograph of the test apparatus used for the erosion experiments.

Fig. 3. Schematic drawing of the erosion tester.

Fig. 4. (A) A drawing of the velocity calibration equipment and the modified test apparatus. (B) Parameters measured for determining particle velocity.

Fig. 5. (A) Single particle damage caused by 1100 μm diameter SiC at 10° angle of impingement with initial velocity of 67 m/s on 1100-0 aluminum. (B) Profile of impact through approximate centerline of crater. (C) Stereo photographs of impact (use stereo viewer provided in Metals Handbook, Vol. 9).

Fig. 6. (A) Silicon carbide particle (1100 μm diameter) struck the 1100-0 aluminum specimen at 67 m/s at $\alpha = 11°$ causing the crater shown. (B) Profile of impact taken along section line X-X. (C) Stereo pair of damage (use viewer provided in Metals Handbook, Vol. 9).

Fig. 7. (A) Impact damage on 1100-0 aluminum the result of a single 1100 μm diameter. SiC particle with initial velocity of 67 m/s and at angle of incidence of 15°. (B) Crater profile along section X-X. (C) Stereo photographs (use viewer provided in Metals Handbook, Vol.9).

Fig. 8. (A) Damage of 1100-0 aluminum specimen due to 1100 μm diameter. SiC particle at $\alpha = 20°$ and initial velocity of 67 m/s. (B) Stereo photographs of damage (use viewer provided in Metals Handbook, Vol. 9).

Fig. 9. (A) Photograph of 1100-0 aluminum specimen damaged by SiC particle with 1100 μm diameter at $\alpha = 30°$ and with initial velocity of 67 m/s.

(B) Crater profile along section X-X. (C) Stereo view of impact crater (use viewer provided in Metals Handbook, Vol. 9).

Fig. 10. (A) Single impact crater in 1100-0 aluminum the results of SiC particle (1100 μm diameter) striking the surface at $\alpha = 60°$ and at 67 m/s. (B) Profile of crater through approximate centerline. (C) Stereo pairs of damage (use viewer found in Metals Handbook, Vol. 9).

Fig. 11. (A) Damage to 1100-0 aluminum specimen due to 1100 μm diameter SiC particle with angle of impingement of 90° and initial velocity of 67 m/s. (B) Profile of crater through section X-X. (C) Stereo photographs of crater (use viewer provided in Metals Handbook, Vol. 9).

Fig. 12. Plot of normalized erosion as a function of the angle of incidence, and also shown is velocity exponent n for several angles.

Fig. 13. Normalized experimental and predicted erosion (g/g) results as a function of the angle α.

Fig. 14. Plot of erosion per particle (gm/part) as a function of angle of incidence (α) for experimental and predicted results.

Fig. 15. Single particle crater profiles found experimentally and predicted for $\alpha = 10°$.

Fig. 16. Plot of crater profiles found experimentally and predicted by the analysis for $\alpha = 30°$.

Fig. 17. For single impacts, a plot of the predicted plastic flow stress as a function of the angle α.

Fig. 18. Weight loss (gms) plotted as a function of the amount of SiC abrasive.

Fig. 19. Plot of erosion (gms) as a function of the amount of silicon carbide abrasive.

Fig. 20. (A) Two-dimensional picture of angular particle removing material. (B) Forces acting on particle during material removal process as used in the modified analysis. (C) Location of forces acting on particle assuming an included angle of about 120°.

Fig. 21. Single particle crater profiles for representative experimental results and profiles predicted by original and modified analysis at (A) $\alpha = 10$ and (B) $\alpha = 30°$. Results are scaled such that the maximum depth of cut for experimental and predicted results are equal for a given α. Experimental curves correspond to the dash-dot curves in Fig. 15 and 16.

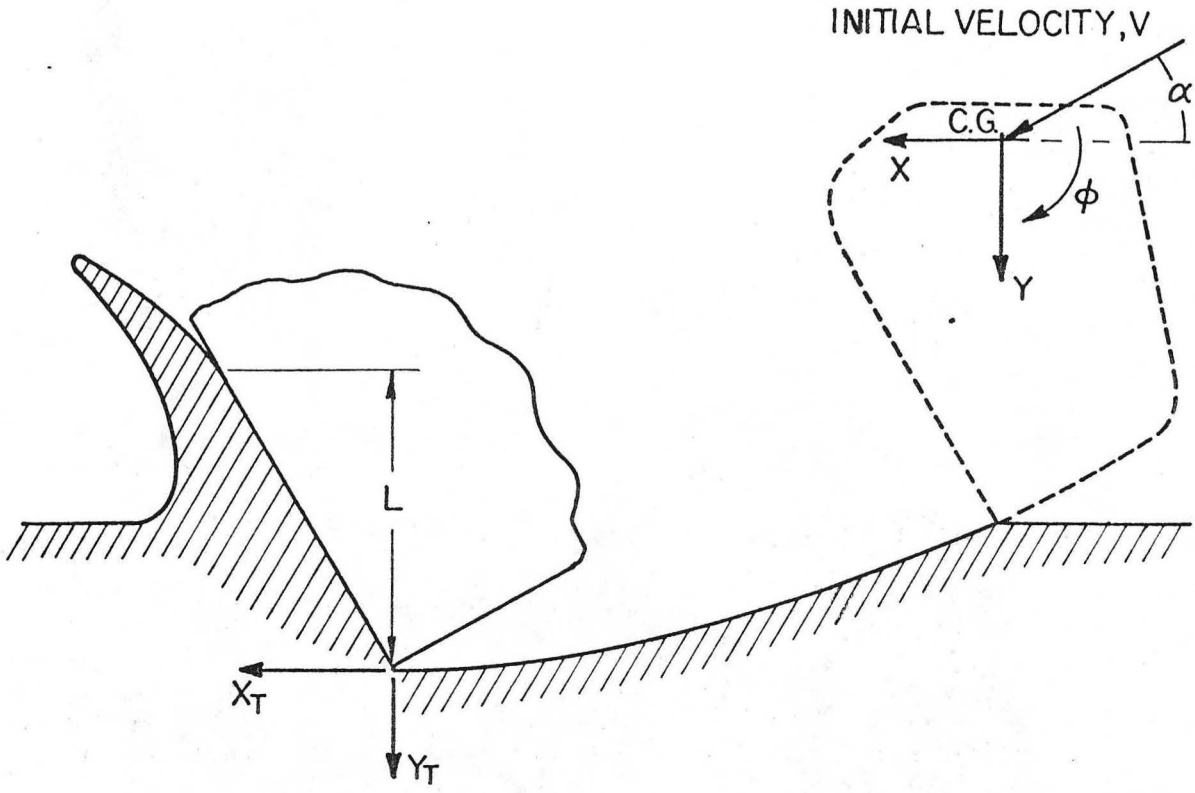

A

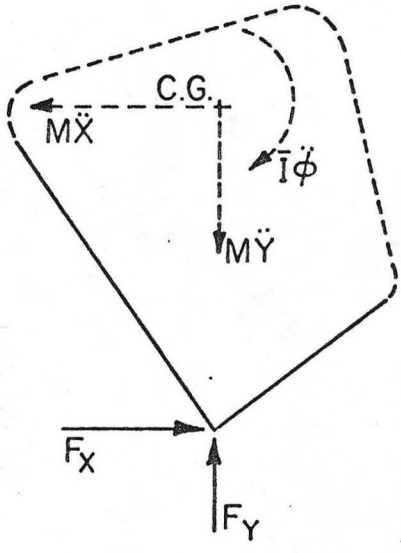

B

X = X-COORDINATE OF C.G.
Y = Y-COORDINATE OF C.G.
ϕ = PARTICLE ROTATION
$X_T \cong X + R\phi$
$Y_T \cong Y$
m = MASS OF PARTICLE
I = MOMENT OF INERTIA
b = WIDTH OF CONTACT FACE
R = RADIUS OF PARTICLE
$k = F_Y / F_X$
$\psi = L/Y_T$
V = INITIAL VELOCITY
α = ANGLE OF INCIDENCE

XBL775-5526

Fig. 1

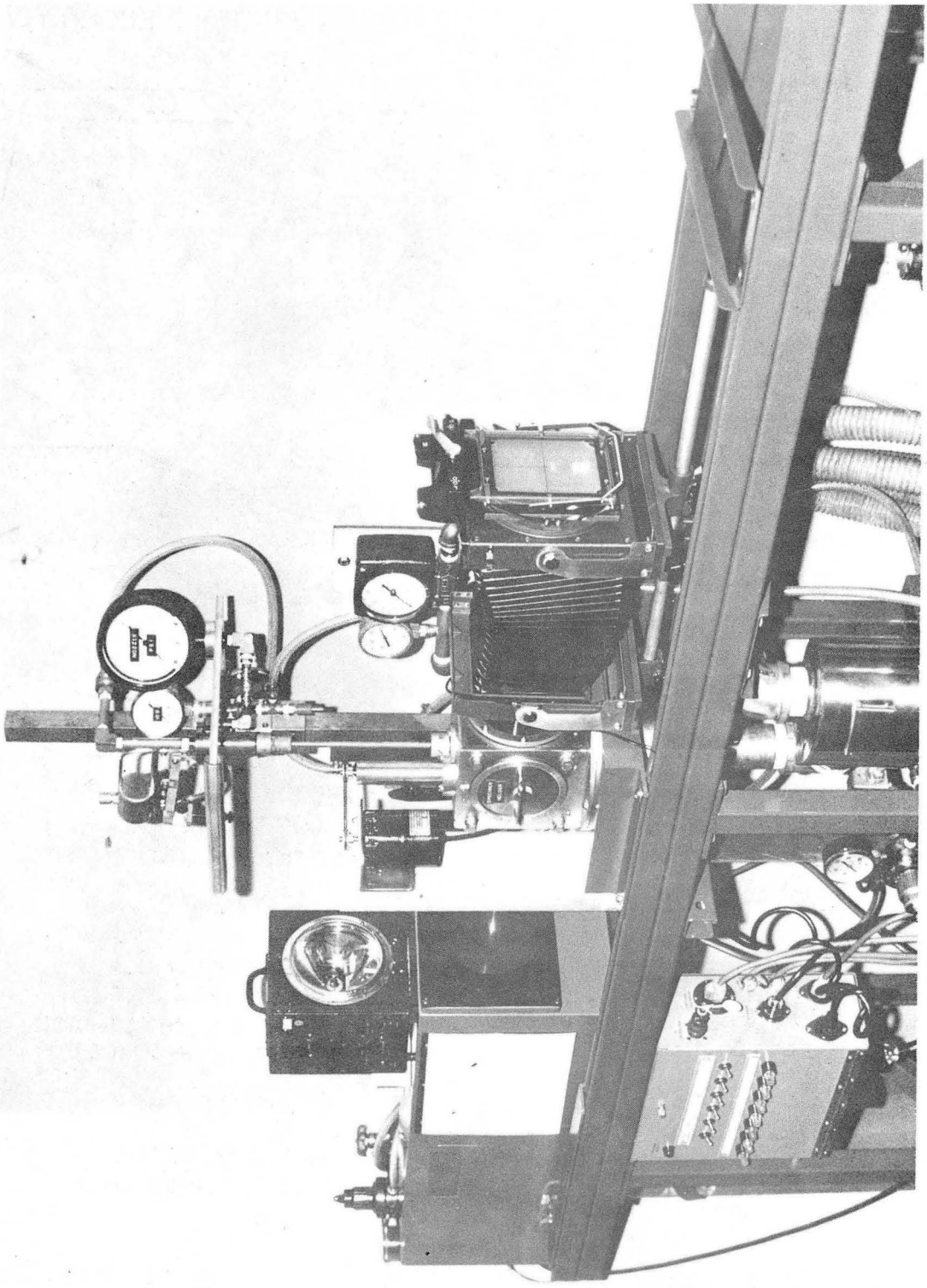

Fig. 2

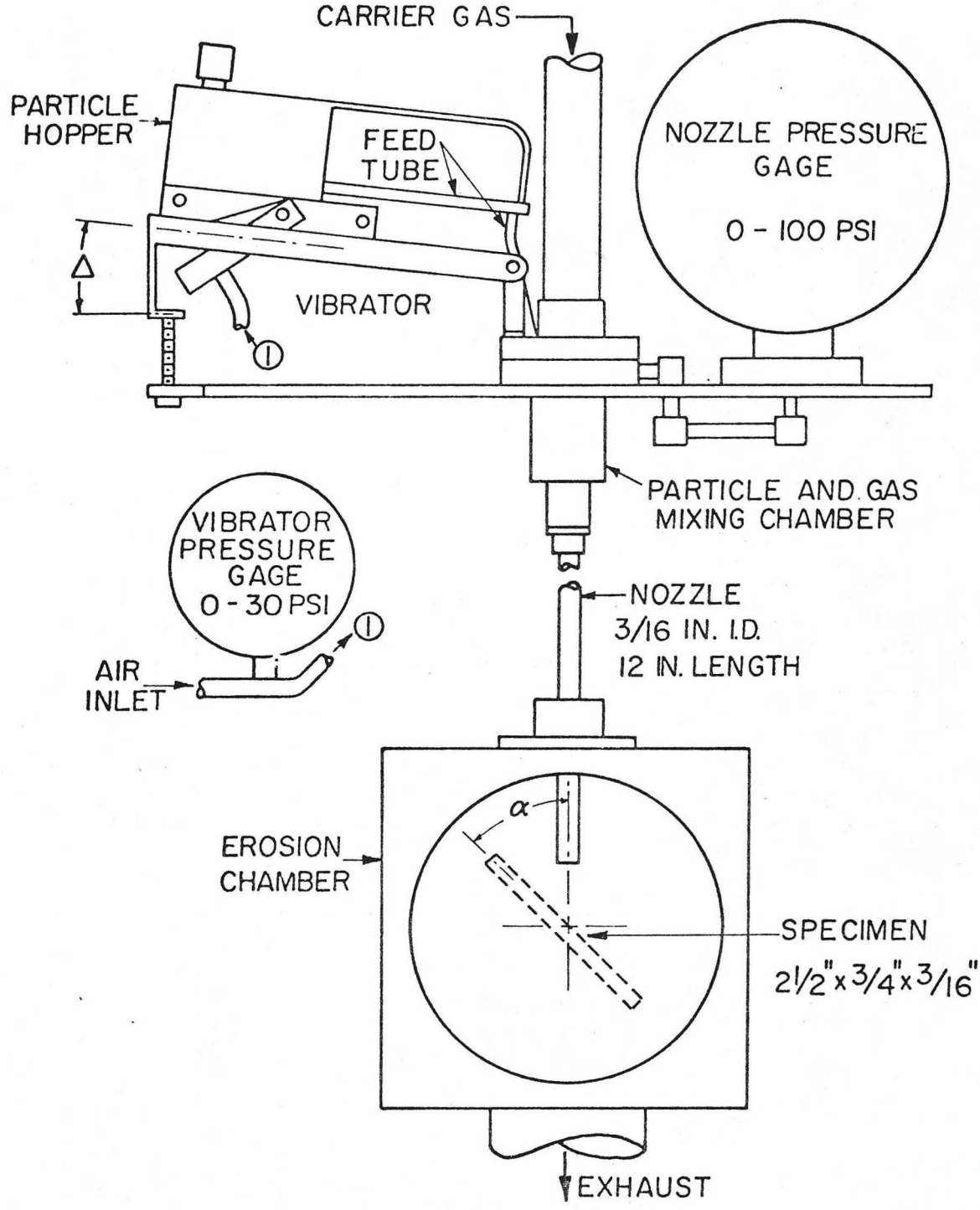

Fig. 3

XBL775-5525

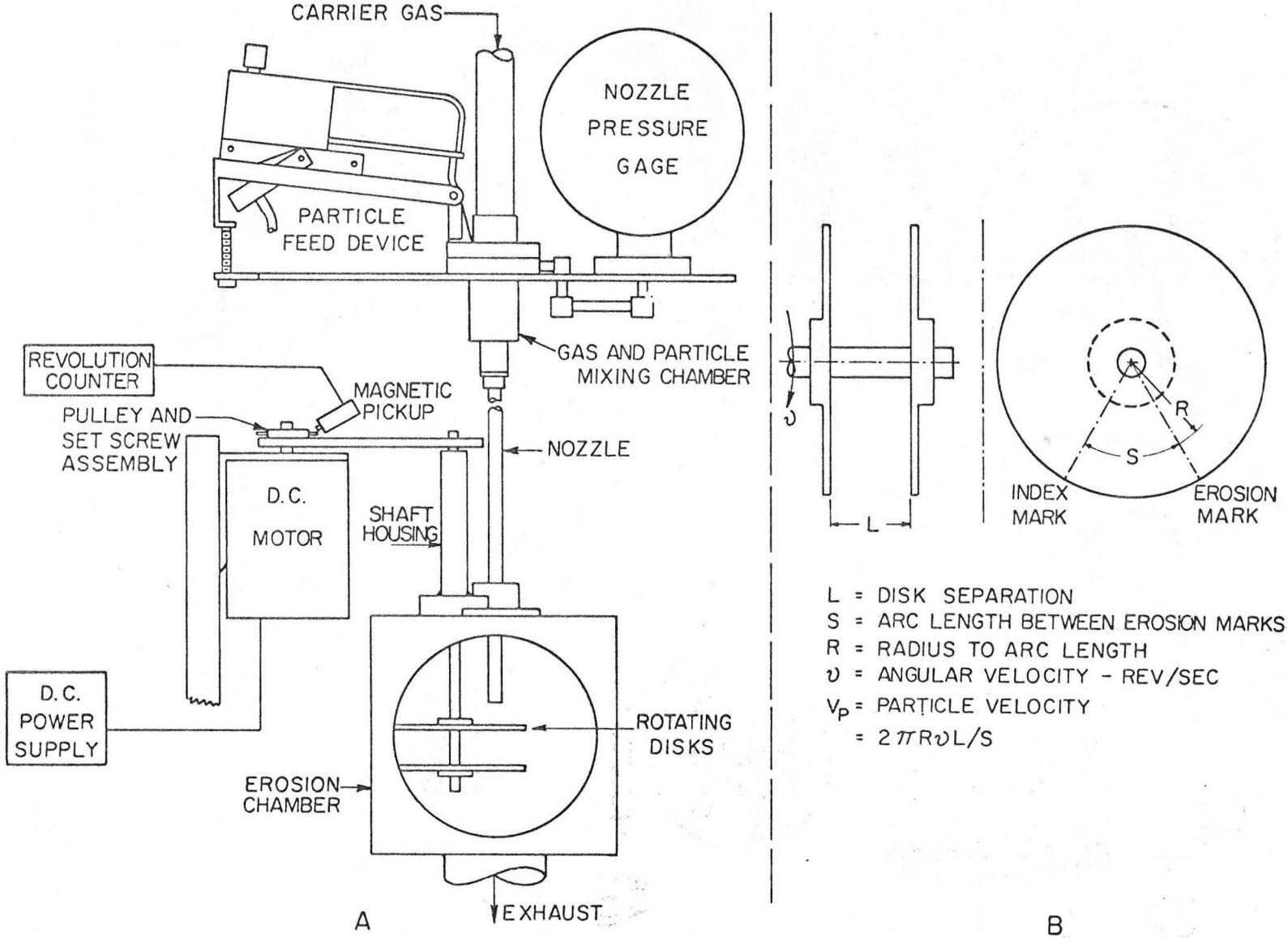

L = DISK SEPARATION
S = ARC LENGTH BETWEEN EROSION MARKS
R = RADIUS TO ARC LENGTH
υ = ANGULAR VELOCITY - REV/SEC
V_p = PARTICLE VELOCITY
$= 2\pi R\upsilon L/S$

Fig. 4

XBL 775-5524

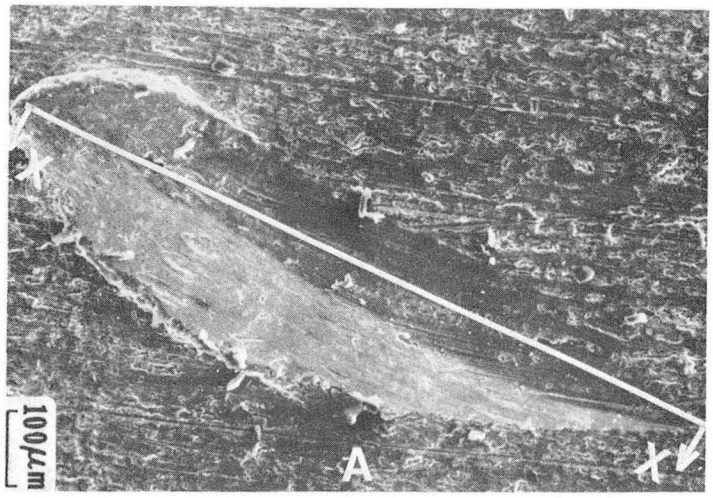

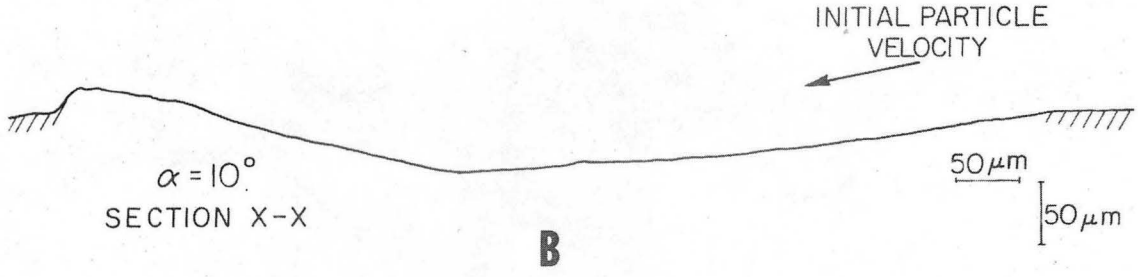

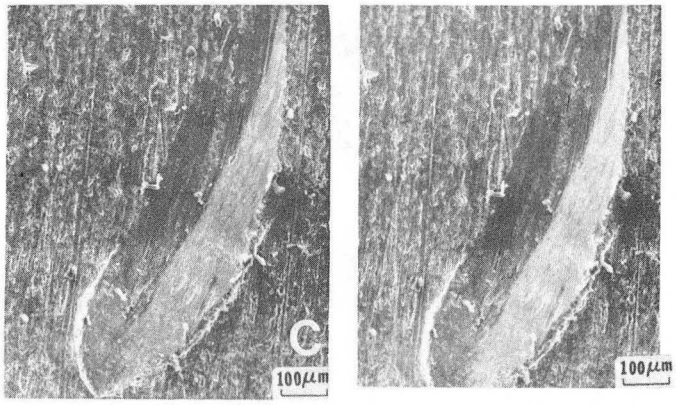

Fig. 5

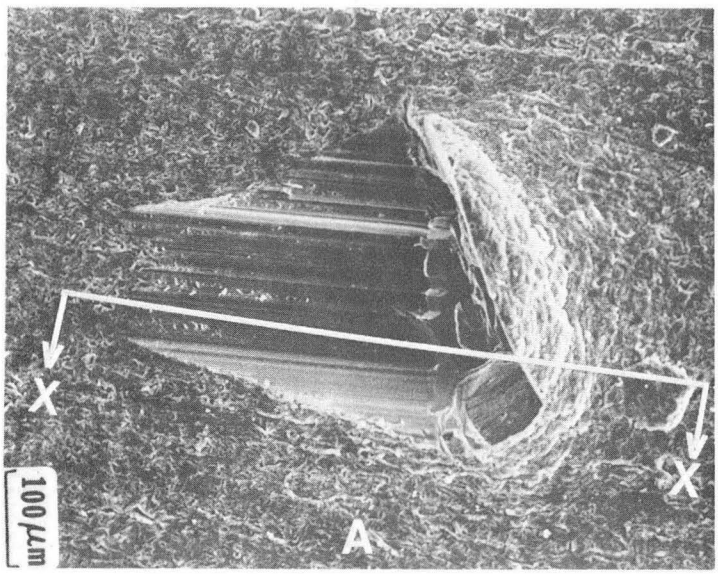
X
X
100 μm
A

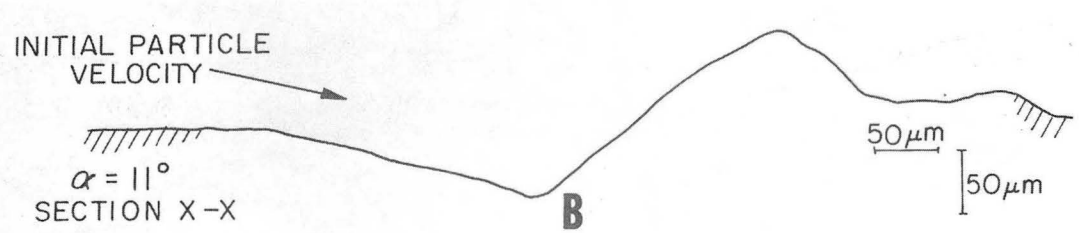
INITIAL PARTICLE
VELOCITY
α = 11°
SECTION X-X
B
50μm
50μm

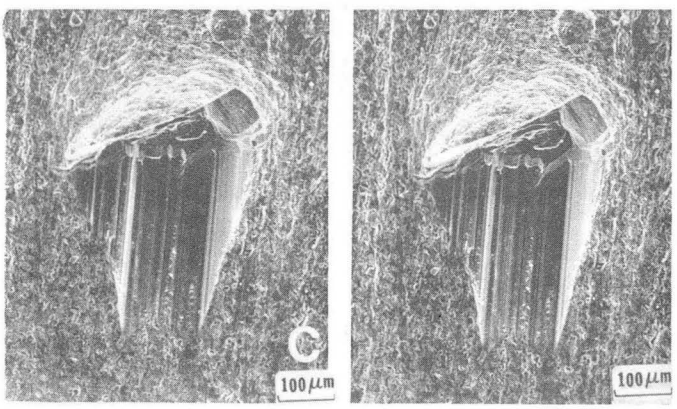
100 μm
100 μm

Fig. 6

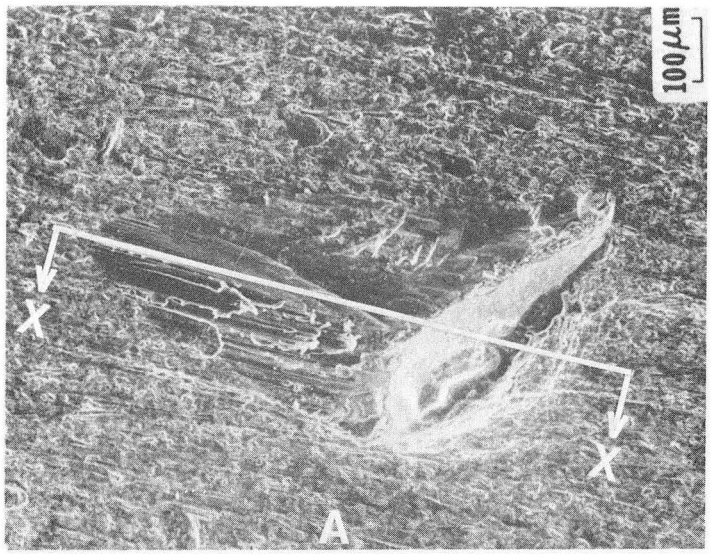

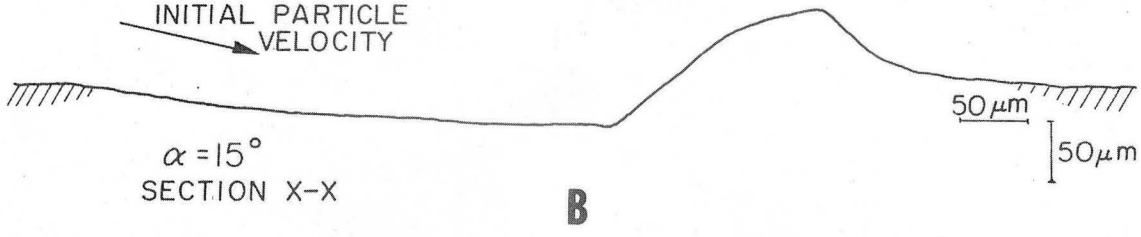

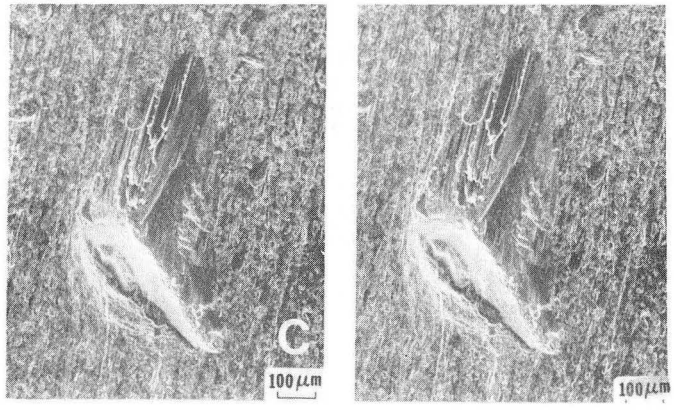

Fig. 7

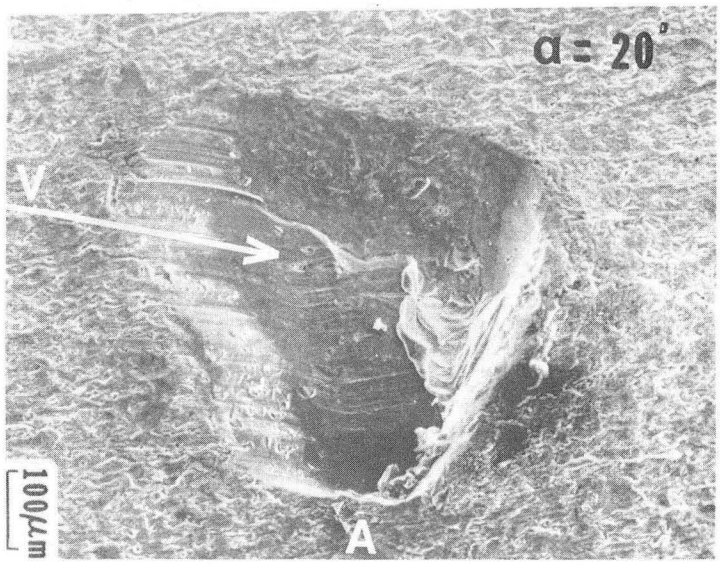

Fig. 8

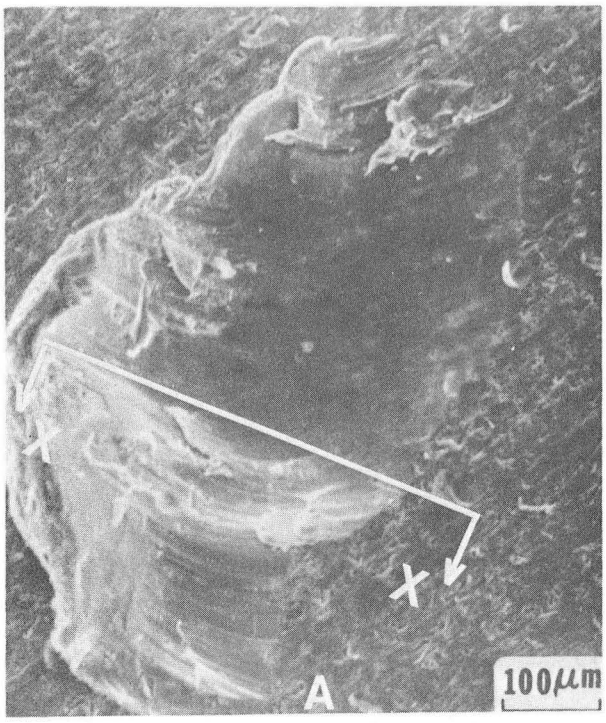

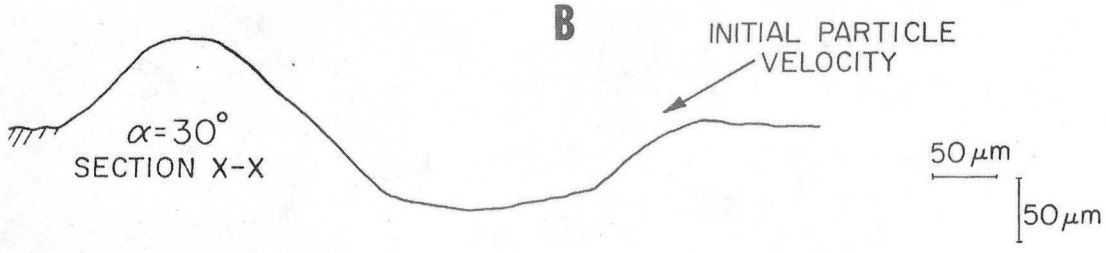

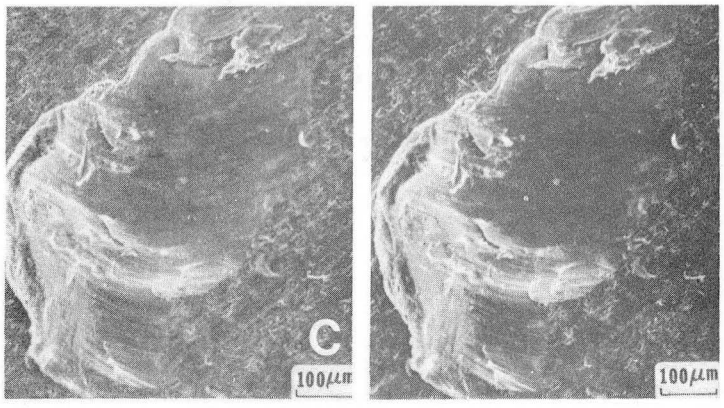

Fig. 9

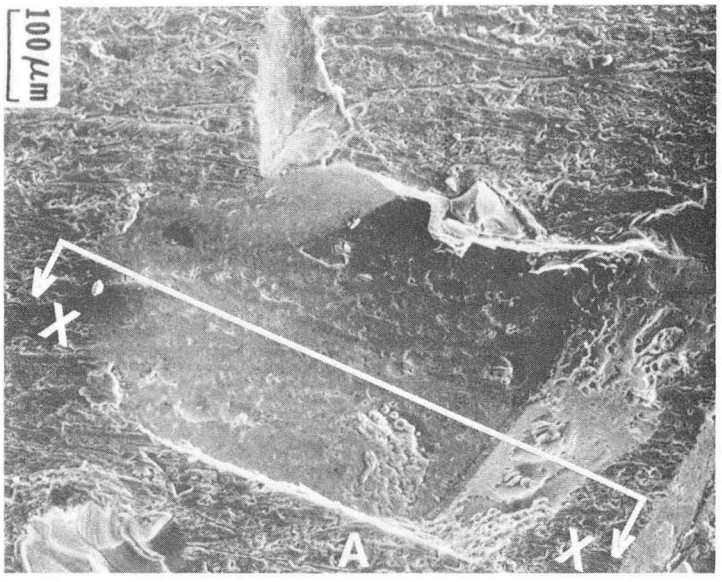
100 μm
X
X
A

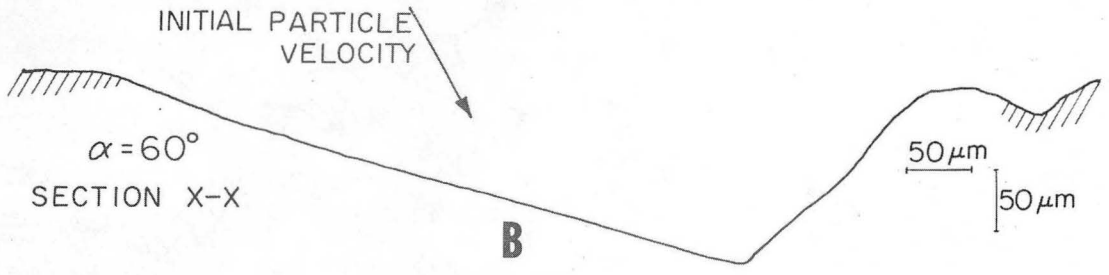
INITIAL PARTICLE
VELOCITY
α = 60°
SECTION X-X
B
50 μm
50 μm

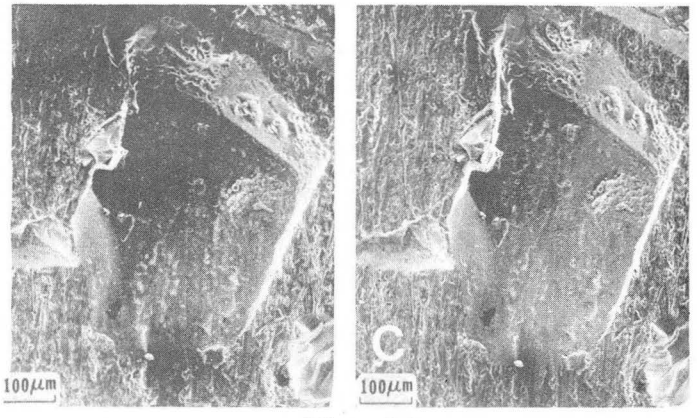
100μm
C
100μm

Fig. 10

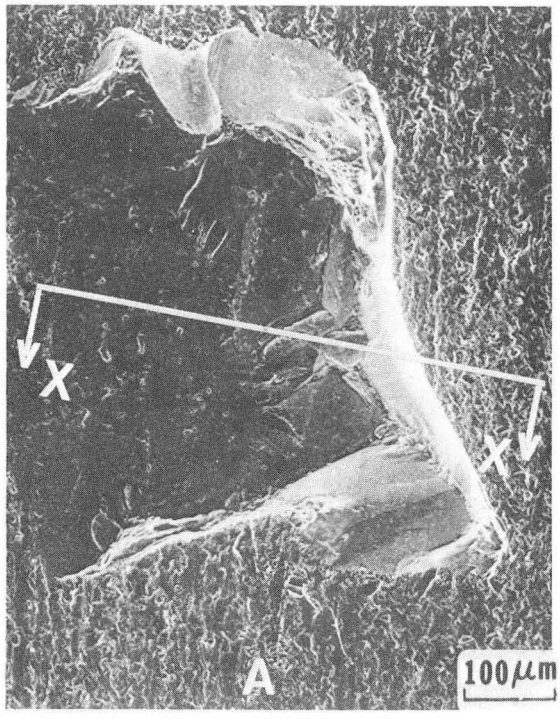

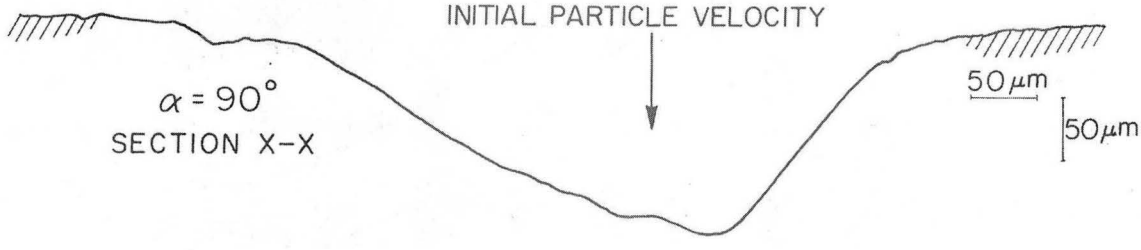

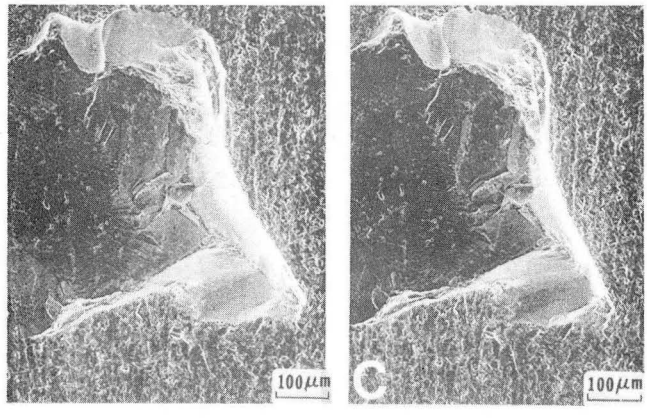

Fig. 11

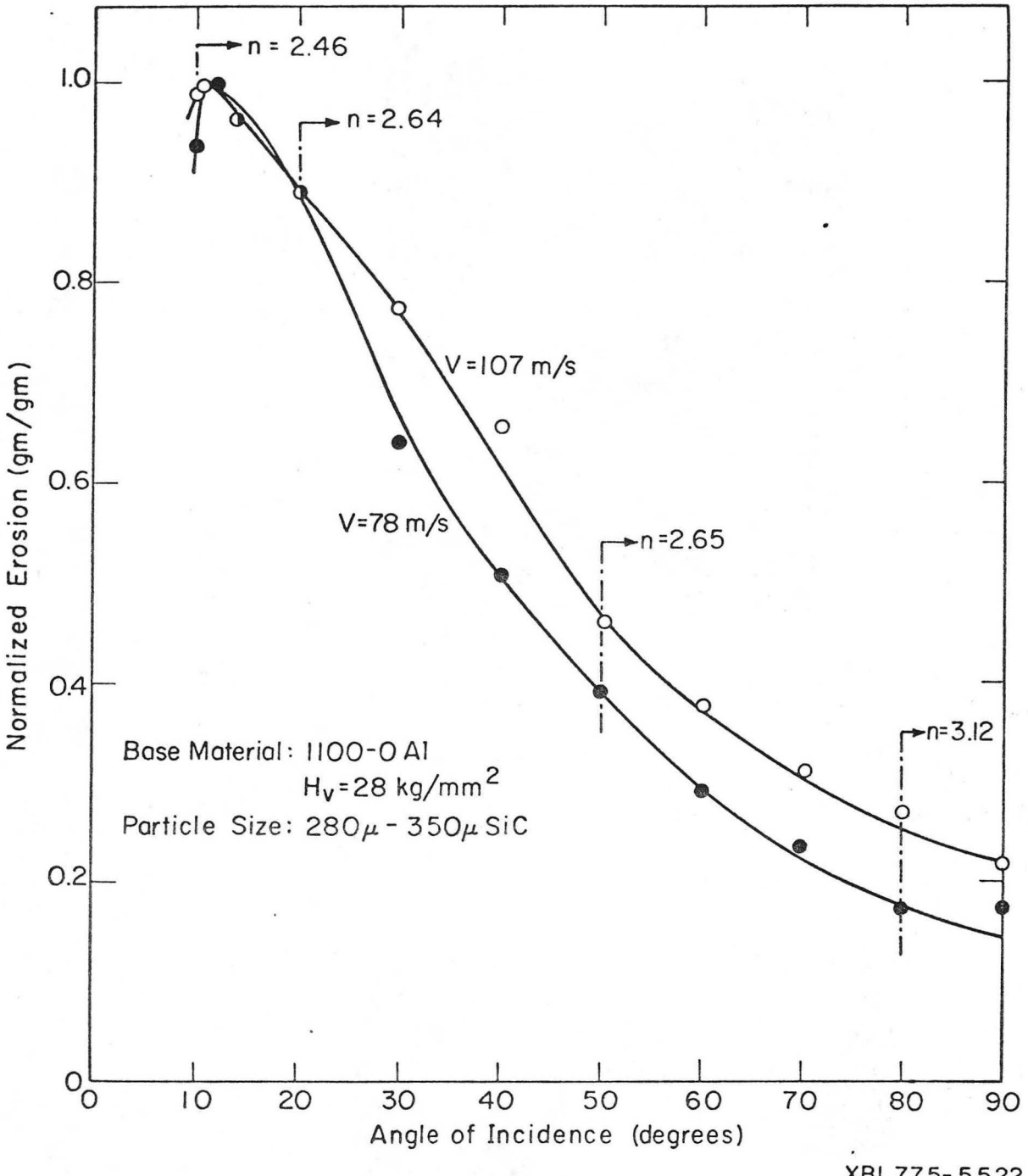
n = 2.46
n = 2.64
n = 2.65
n = 3.12
V = 107 m/s
V = 78 m/s
Base Material: 1100-0 Al
H_V = 28 kg/mm^2
Particle Size: 280μ - 350μ SiC
Normalized Erosion (gm/gm)
Angle of Incidence (degrees)
0
0.2
0.4
0.6
0.8
1.0
0
10
20
30
40
50
60
70
80
90
XBL775-5522

Fig. 12

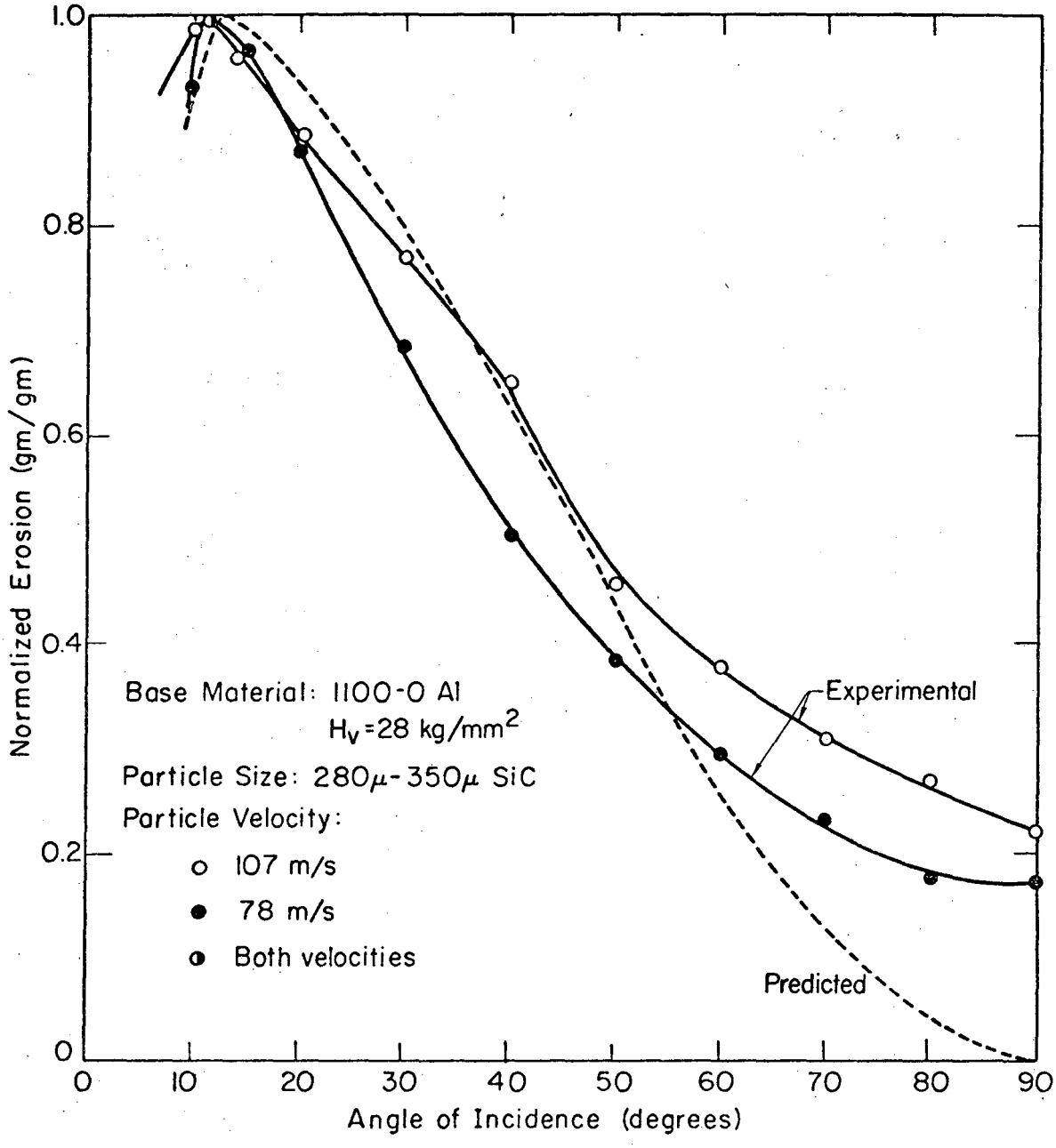

XBL775-5521

Fig. 13

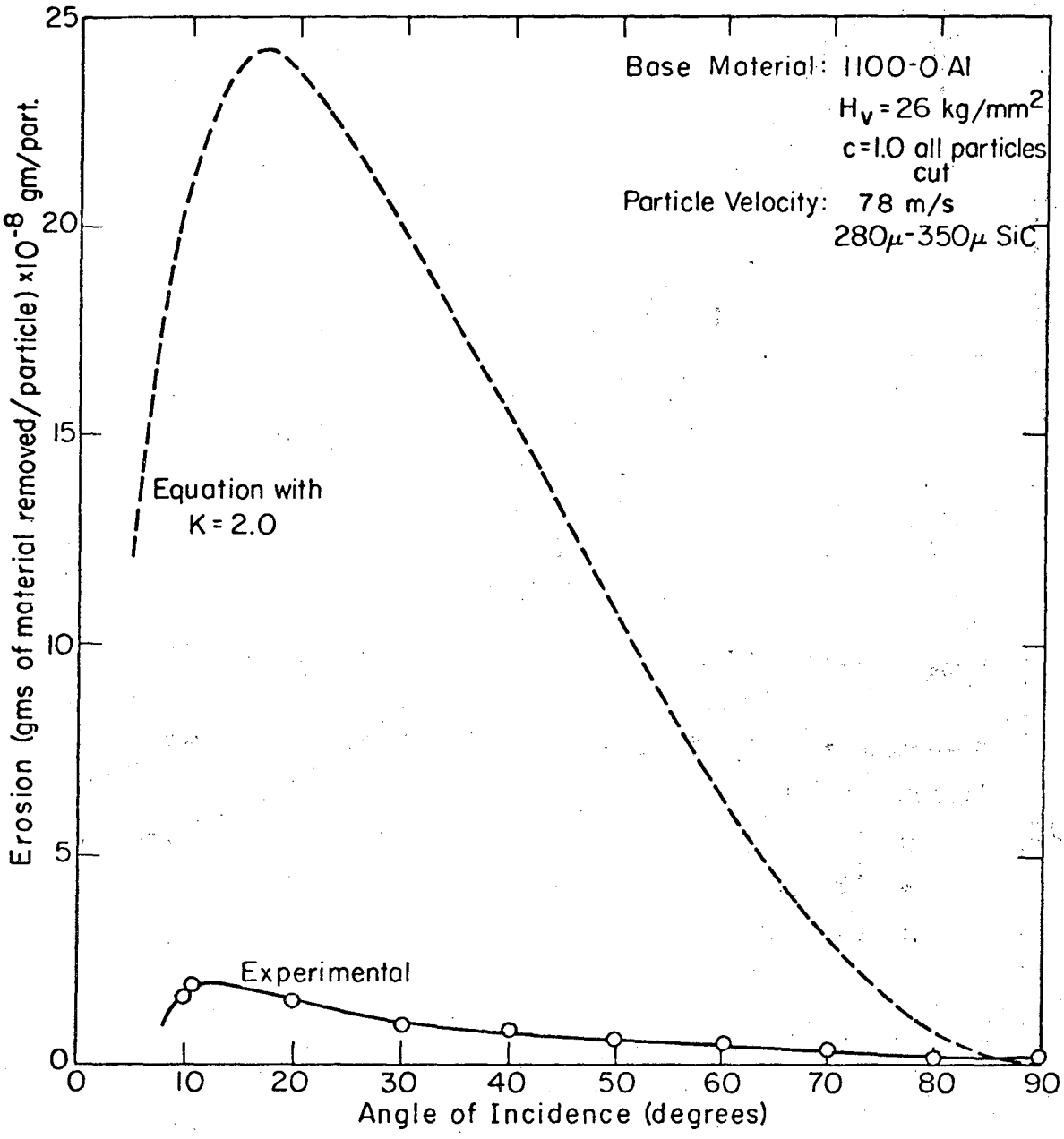

Fig. 14

XBL 775-5523

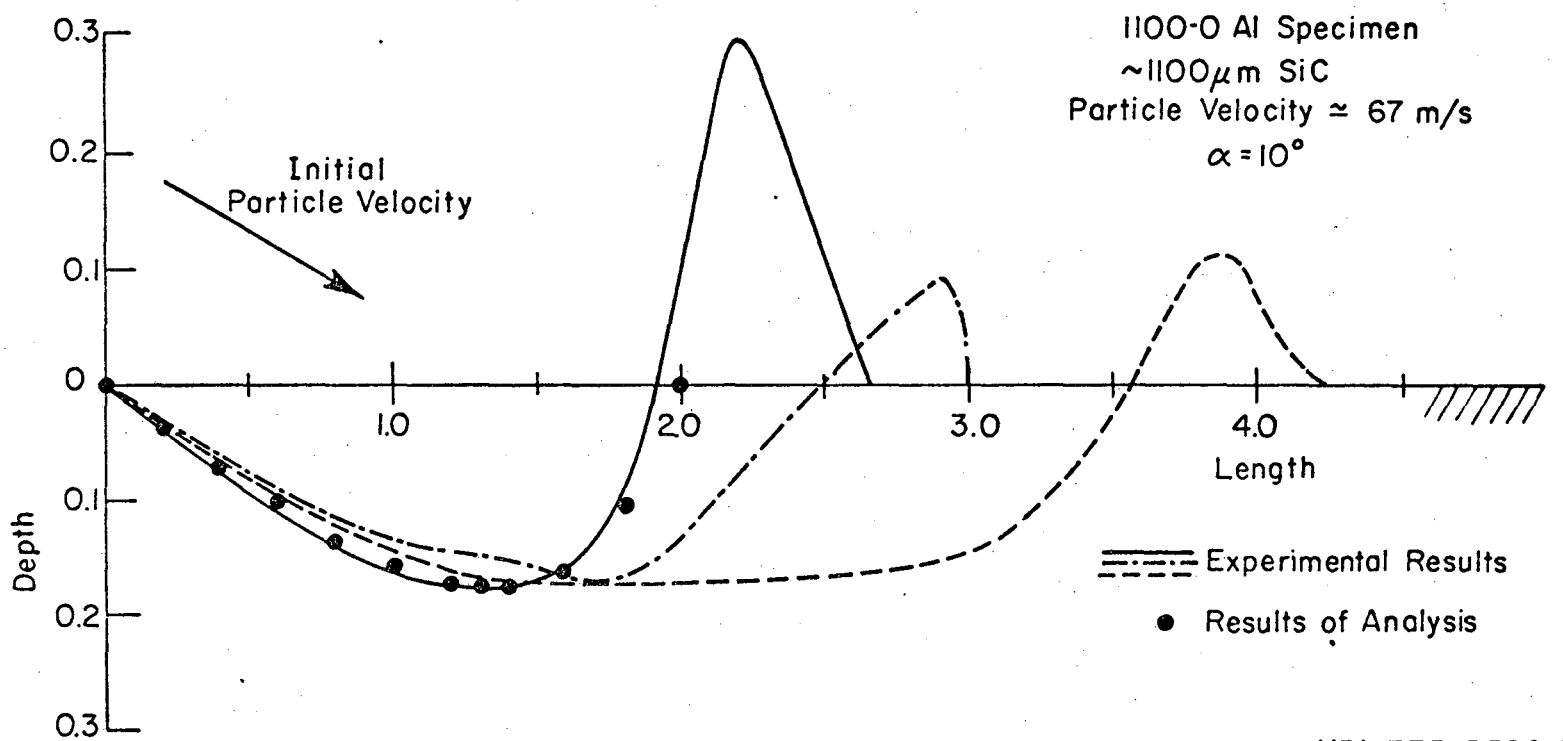

Fig. 15

XBL 775-5528

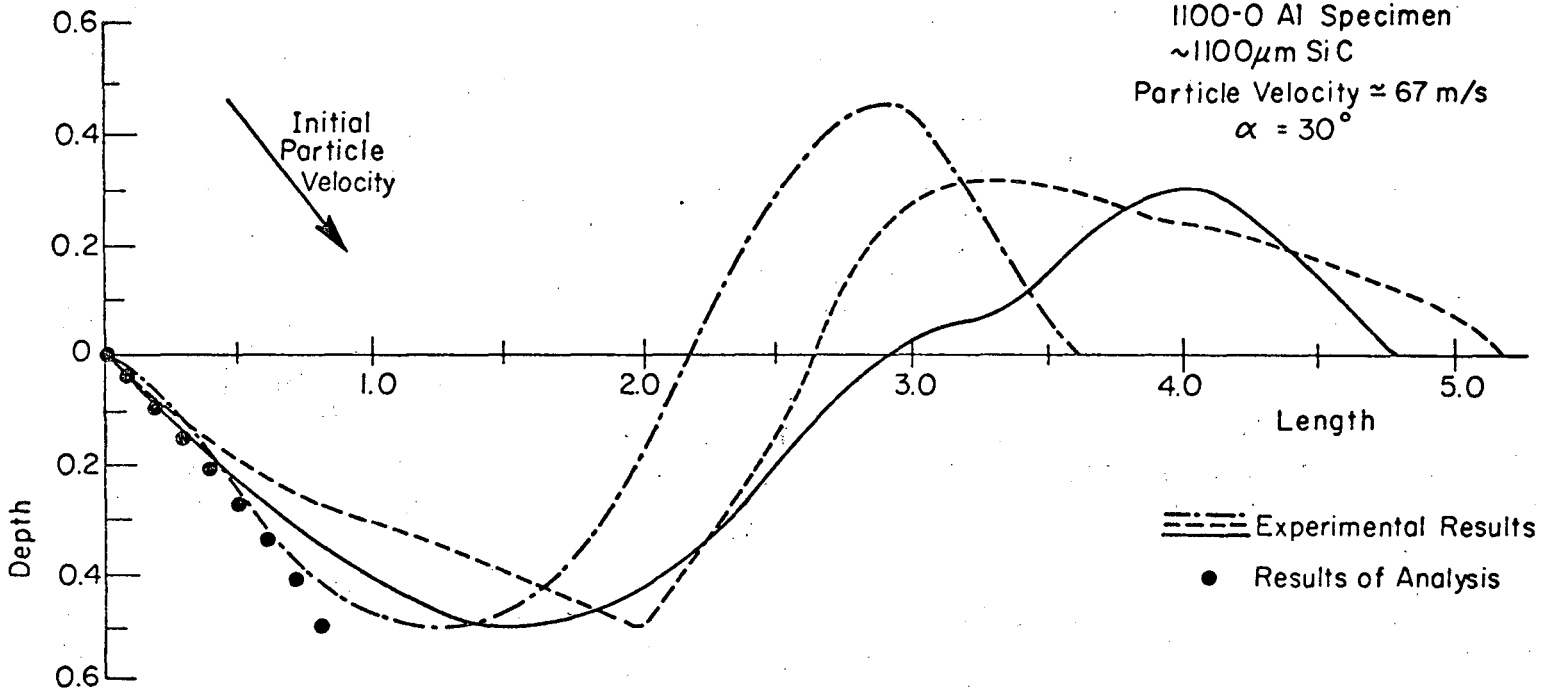

Fig. 16

XBL775-5529

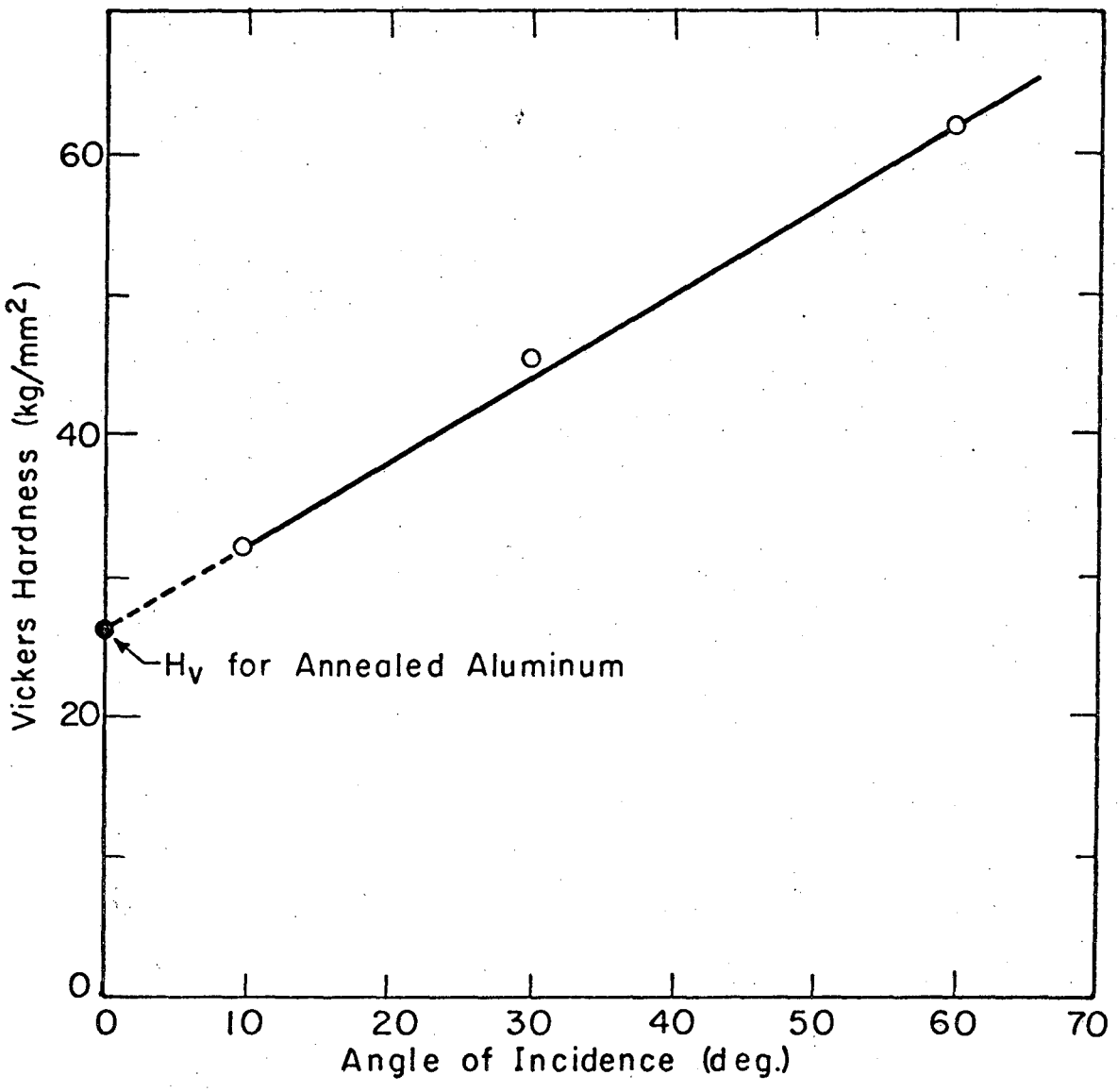

Fig. 17

XBL775-5519

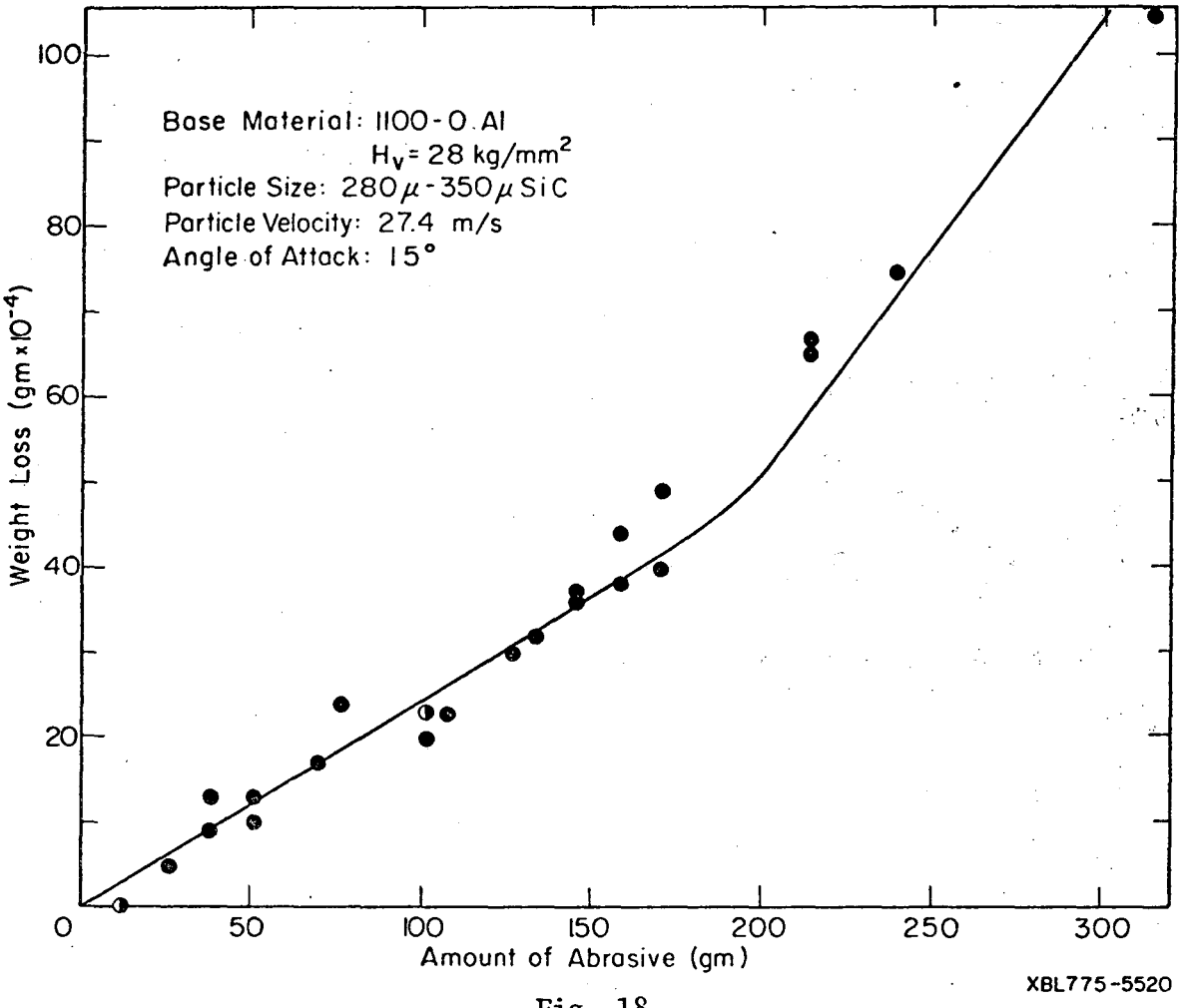
Base Material: 1100-O Al
H_V = 28 kg/mm^2
Particle Size: 280μ-350μ SiC
Particle Velocity: 27.4 m/s
Angle of Attack: 15°
Weight Loss (gm x 10^{-4})
Amount of Abrasive (gm)
0
20
40
60
80
100
50
100
150
200
250
300
XBL775-5520

Fig. 18

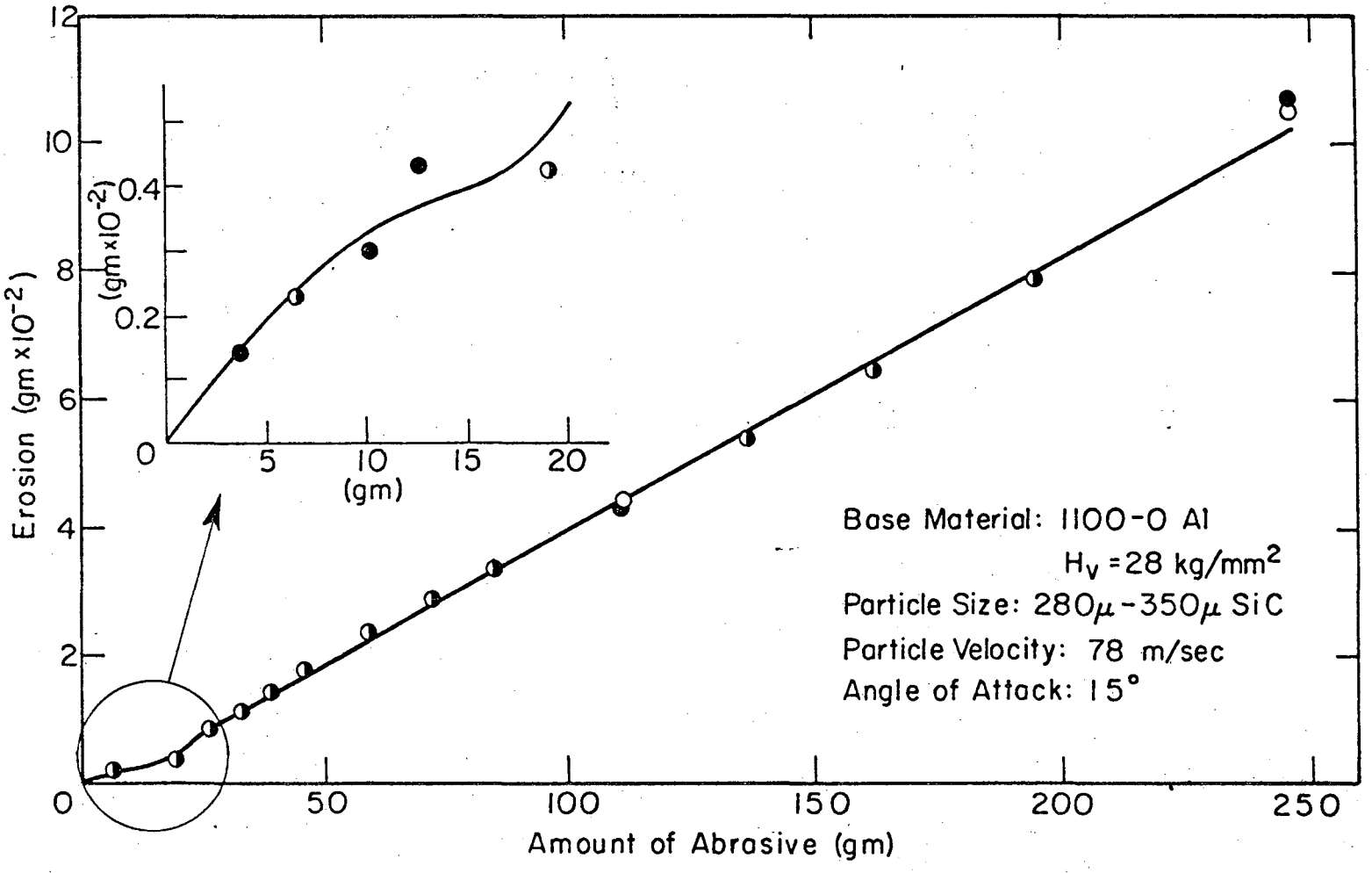

Fig. 19

XBL775-5518

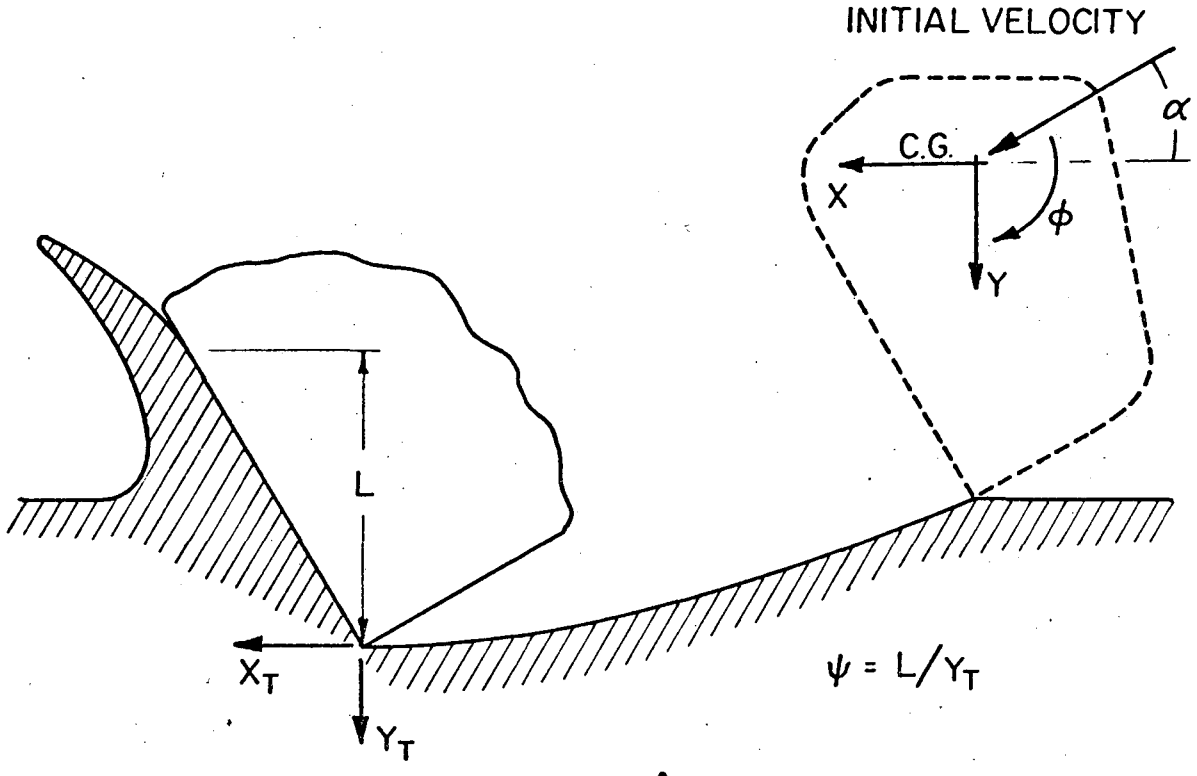

A

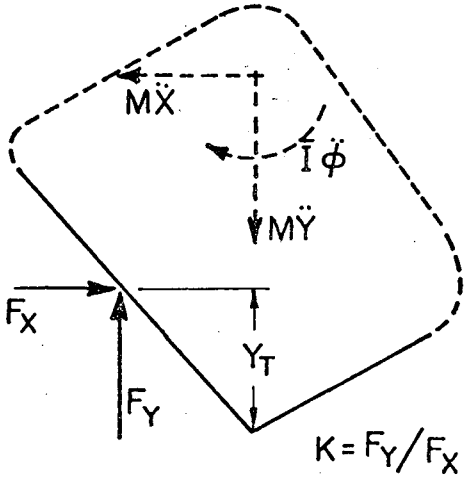

B

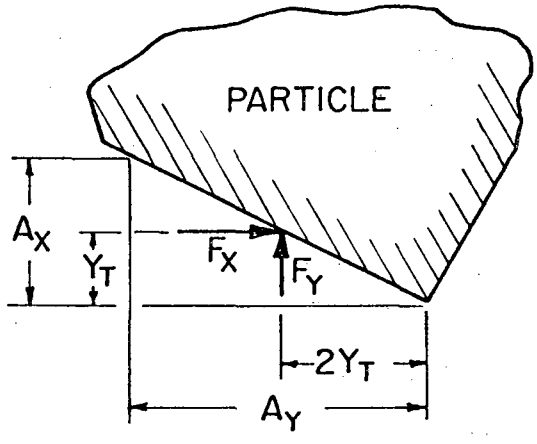

A_Y = PROJECTED CONTACT AREA

A_X = PROJECTED AREA X-DIR.

C

XBL775-5527

Fig. 20

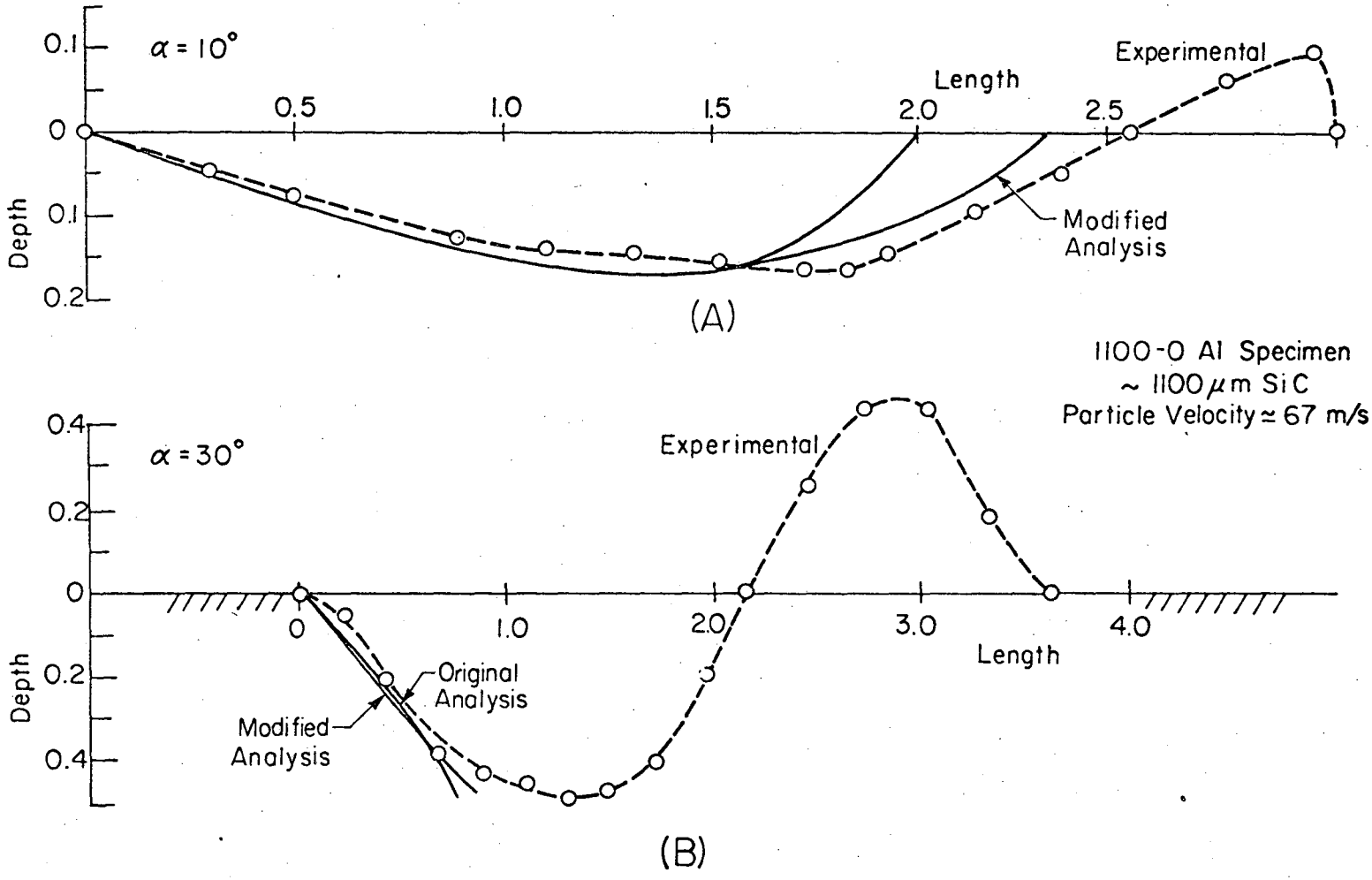

Fig. 21

XBL775-5530

TECHNICAL INFORMATION DIVISION
LAWRENCE BERKELEY LABORATORY
UNIVERSITY OF CALIFORNIA
BERKELEY, CALIFORNIA 94720